Chapter 4

Solutal Marangoni Convection: Mass Transfer Characteristics

4.1 Introduction

In chapter 2, the microgravity experiments with V-shaped containers have been described. In chapter 3, the evolution of Marangoni flow and concentration patterns in these V-shaped containers have been modelled numerically. A reasonable agreement between experiment and model was obtained. In this chapter, the model that has been developed in chapter 3 is used to predict mass transfer characteristics for gas-liquid systems with a non-deformable interface. That is, the influence of Marangoni convection on the gas-liquid mass transfer is examined. In this way, an attempt is made to establish a link between the microgravity experiments and a better understanding of the relation between the Marangoni effect and mass transfer. The parameters varied in this study are the Marangoni, Schmidt and Biot numbers.

Literature review

Experimentally, the influence of the Marangoni effect on the mass transfer coefficient in gas-liquid systems has been studied by several authors [1, 2, 3, 4, 5, 6, 7]. In the most relevant studies [2, 5, 7], the enhancement of the liquid side mass transfer coefficient k_L was correlated by equations of the following type:

$$\phi = \frac{k_L}{k_L^*} \qquad (1)$$

$$\phi = \left(\frac{Ma}{Ma_C} \right)^n \qquad (2)$$

In these equations ϕ is the enhancement factor, k_L^* the liquid side mass transfer coefficient in the absence of interfacial turbulence, Ma the Marangoni number, Ma_c the critical Marangoni number, and n an empirical parameter. Equation (2) is only valid when $Ma > Ma_c$. For values of Ma smaller than Ma_c, the enhancement factor is equal to 1. Grymzin et al. used another equation for ϕ [6].

$$\phi = 1 + K\,Ma \qquad (3)$$

K in this equation is an empirical parameter, which depends on the gas to liquid resistance ratio. Semkov and Kolev argue in their theoretical review [8] that this equation is

less convenient, as K depends on the Marangoni number as well as on the type of contacting equipment.

The Marangoni number was not defined in the same way by all of the authors. Actually, three different definitions were used.

$$Ma_B = \frac{(\gamma_i - \gamma_B)}{\mu\, k_L^*} \tag{4}$$

$$Ma_{Gr} = \frac{(\gamma_i - \gamma_B)\, H_L}{\mu\, D} \tag{5}$$

$$Ma_W = \frac{\left(-\frac{\partial\gamma}{\partial c}\right)\left(\frac{c_B^0 - c_i^0}{d}\right) H_L^2}{\mu\, D} \tag{6}$$

In these equations, Ma_B, Ma_{Gr} and Ma_W are the Marangoni numbers used by **B**rian et al. [2] and Imaishi et al. [5], **Gr**ymzin et al. [6], and **W**armuzinski and Buzek [7], respectively, γ_i and γ_B the surface tension corresponding to the concentration at the interface (c_i) and in the liquid bulk (c_B) respectively, μ the dynamic viscosity, D the diffusivity of the solute which influences the surface tension, d the penetration depth and H_L the liquid film thickness. The different definitions obviously result in quantitatively different Marangoni numbers, but if equation (2) is valid for the Brian definition, it is expected to hold for the Grymzin definition as well, provided the film thickness H_L is not influenced by the Marangoni effect. However, in the Warmuzinski definition the initial concentrations are used to calculate the characteristic surface tension difference, rather than the actual concentrations. As this characteristic surface tension difference is influenced by the Marangoni effect, a different value for the parameter n in equation (2) is found, depending on which definition for the Marangoni number is used.

Note that the values of the Marangoni numbers in equations (4) and (5) depend on the actual concentrations, and therefore on the value of the mass transfer coefficient. These equations, combined with equation (2), can therefore not be implemented straightforwardly.

The different authors found different values for the parameter n in equation (2). The values vary roughly between 0.25 and 1. Brian et al. found n = 0.25 for the desorption of acetone in wetted wall columns, n = 0.5 for the desorption of diethyl ether, and n = 1.3 for the desorption of triethylamine [2]. For the absorption of CO_2 in monoethanolamine, Warmuzinski and Buzek determined n to be 0.26 [7]. Imaishi et al. studied the desorption of various solutes in wetted wall columns and liquid jets and calculated n to be 0.4 ± 0.1 [5]. Golovin [9] discovered that Imaishi et al. had made an error in calculating the interfacial concentration and recalculated n for their experiments to be 0.68 ± 0.3.

Brian et al. expected that n would depend on the phase resistance ratio, but did not know what the relationship would be. Imaishi et al. considered their n to be independent of the phase resistance ratio, but Semkov and Kolev nevertheless correlated their (wrongly calculated) data with the phase resistance ratio (Biot number):

$$Bi_R^* = \frac{m\, k_G}{k_L^*} \tag{7}$$

$$n = 0.2\left(\frac{Bi_R^*}{1+Bi_R^*}\right) + 0.27 \tag{8}$$

Golovin put forward an elegant theory in which n does not depend on the Biot number, but on the type of roll cells enhancing the mass transfer [9]. Similar theories have been developed by Rabinovich and co-workers (e.g. [10]). Golovin discriminated between two types of roll cells: chaotic roll cells whose lifetime is of the same order of magnitude as the characteristic time of liquid circulation in a cell (type A), and spatially ordered convective cells (type B). The latter cells would be observed in systems without artificial stirring and with a lifetime that is long enough for regular structures to form. The chaotic roll cells would be typical of stirred cells, moving drops and turbulent films. Golovin derived the following relationship between the Sherwood number for a single roll cell in the liquid phase Sh_L and the Marangoni number $Ma_{G,L}$ for type A cells.

$$Sh_L = b^2\, Ma_{G,L}\, Sc^{-1/2} \tag{9}$$

$$Sh_L = \frac{j H}{D(c_B - c_i)} \tag{10}$$

$$Ma_{G,L} = \frac{\left(-\frac{\partial\gamma}{\partial c}\right)(c_B - c_i)H}{(\mu_L + \mu_G)D} \tag{11}$$

In these equations, b is an empirical parameter characterising the extent of surface renewal in a roll cell, Sc is the Schmidt number, j the interfacial mass flux, and H a characteristic length for mass transport. The equations are valid for $Ma > Ma_c$. The equations show that for chaotic roll cells the parameter n equals 1. For type B roll cells, the following expression for Sh_L can be obtained, if Golovins expression (10) is modified slightly.

$$Sh_L = b^{4/3}\, Ma_{G,L}^{1/3}\, Sc^{1/6}\left(\frac{H}{L}\right)^{2/3} \tag{12}$$

In this expression, L is the characteristic length scale of the roll cell. In his paper, Golovin uses L as a length scale in the definition of both the Sherwood number and the Marangoni number in the equation above. He assumes implicitly L is not dependent on the Marangoni effect, and this is not necessarily true. Therefore, the equation stated above is more appropriate. Provided L does not depend on the extent of the Marangoni effect, but only on the geometry of the system, the parameter n assumes the value 1/3 for type B roll cells. In most cases, however, L does depend on the Marangoni number. The results of chapter 3 indicate that in a system confined by solid walls the value of L is larger the larger the Marangoni number is, and n would therefore be smaller than 1/3.

Golovin continues to argue that the different values of n found by different authors correspond to the evolution of different types of roll cells. In laminar wetted wall columns n is closer to 1/3 (e.g. n = 0.25 for desorption of acetone in a wetted wall column) and for turbulent stirred cells or moving drops n is closer to 1 (e.g. desorption of acetone from stirred cells [3]). Most of the experiments corroborate his argument. However, no explanation is presented for n varying between 0.25 and 1.3 in the work of Brian et al. [2]. These different values of n were all obtained with the same low Reynolds number wetted wall column.

For gas-liquid systems, Golovin also sets out to derive an expression for the overall Sherwood number as a function of the Marangoni number $Ma^0_{G,L}$ and the phase resistance ratio. For type A cells, the following expression is obtained (for $Ma > Ma_c$).

$$Sh = \left[\left(\frac{1}{4} \frac{r^2}{b^2 \, Ma^0_{G,L}} + r \right)^{1/2} - \frac{r}{2 b \sqrt{Ma^0_{G,L}}} Sc^{1/4} \right]^2 \tag{13}$$

$$Sh = \frac{j H}{D c^0_B} \tag{14}$$

$$Ma^0_{G,L} = \frac{\left(-\frac{\partial \gamma}{\partial c} \right) c^0_B H}{(\mu_L + \mu_G) D} \tag{15}$$

$$r = \frac{m k_G H}{D} \tag{16}$$

In these equations r is a kind of phase resistance ratio, and m the distribution coefficient. For $r/Ma^0_{G,L} \to \infty$ equation (13) reduces to equation (9), while for $r/Ma^0_{G,L} \to 0$ the Sherwood number is equal to r. For very intensive Marangoni convection the mass transfer is limited by the gas phase mass transfer, while for moderate and small Marangoni convection the mass transfer is limited by the convective mass transport, provided the mass transfer in the liquid phase is still larger than the diffusive mass transfer. Equation (13) is plotted in figure 1 for various values of r and Sc. To plot the equation, the parameter b expressing the surface renewal rate (equation (9)) has been set to 1. It should be noted that for the limit of very intensive Marangoni convection the gas phase mass transfer coefficient is enhanced as well. That is, r is not a constant, but r depends on the Marangoni number as well. Furthermore, for small Marangoni numbers, the Sherwood number is underestimated as the mass transfer in the absence of convection is neglected in these equations.

Also for type B cells, Golovin derives an expression. This expression (expression (37) in Golovins paper), however, is erroneous with respect to the Schmidt number. The correct expression is:

$$Sh = r \, S_B(m_B) \tag{17}$$

$$m_B = \frac{r^3}{b^4\, Sc^{1/2}\, Ma_{G,L}^{0}} \left(\frac{L}{H}\right)^2 \tag{18}$$

The function $S_B(m_B)$ is defined as the solution to the following equation:

$$\left(1 - S_B\right)^4 - m_B\, S_B^3 = 0 \tag{19}$$

Equation (17) reduces to equation (12) for large values of m_B. For small values of m_B (intensive Marangoni effect) equation (17) reduces to Sh = r. Equation (17) is plotted in figure 2 for various values of r and Sc. The ratio (L/H) and b are assumed to be equal to 1.

With respect to the Schmidt number, the trend for type A roll cells is more or less opposite to the trend for type B cells. That is, for type A roll cells the Sherwood number is larger the smaller the Schmidt number is, and for type B roll cells the Sherwood number is larger the larger the Schmidt number is. However, with respect to the liquid phase diffusivity, trends are similar for both types of roll cells. This can easily be seen when the Marangoni number is defined differently.

$$Ma_{G,L}^{n} = \frac{Ma_{G,L}}{Sc} = \frac{\left(-\frac{\partial\gamma}{\partial c}\right)\left(c_B - c_i\right)H}{\left(\mu_L + \mu_G\right)\nu} \tag{20}$$

$$Sh_L = b^2\, Ma_{G,L}^{n}\, Sc^{1/2} \qquad \text{type A roll cells} \tag{21}$$

$$Sh_L = b^{4/3} \left(Ma_{G,L}^{n}\right)^{1/3} Sc^{1/2} \left(\frac{H}{L}\right)^{2/3} \qquad \text{type B roll cells} \tag{22}$$

With this definition of the Marangoni number, the Sherwood number is always proportional to the square root of the Schmidt number, and the mass transfer coefficient proportional with the square root of the liquid phase diffusivity. This definition of the Marangoni number is more consistent with the relevant boundary condition for this problem (equation (21) in chapter 3).

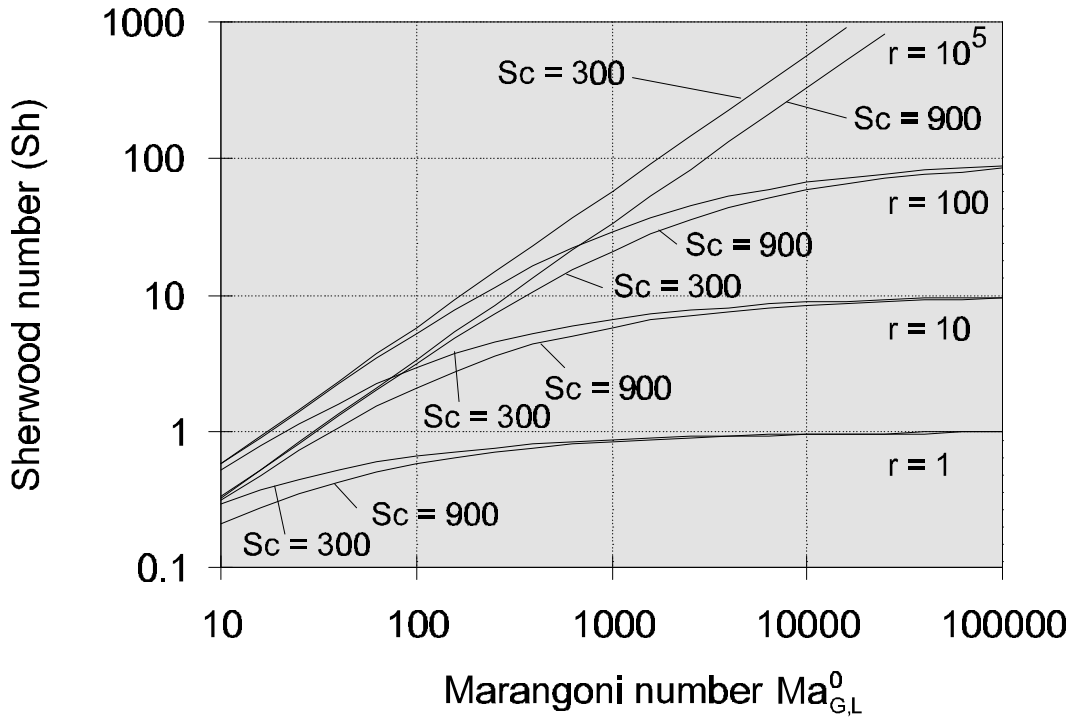

figure 1 *Sherwood number as a function of the Marangoni number $Ma^0_{G,L}$ for type A cells according to equation (13) as derived by Golovin [9] (b = 1).*

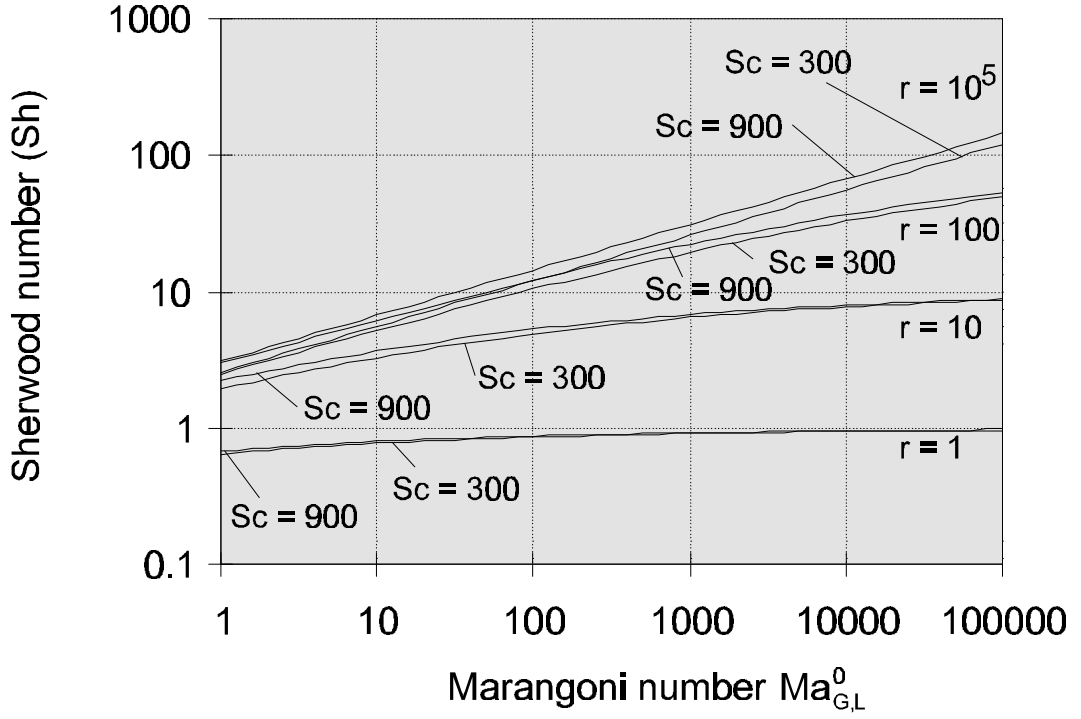

figure 2 *Sherwood number as a function of the Marangoni number $Ma^0_{G,L}$ for type B cells according to equation (17) (b = 1; (L/H) = 1).*

Comparison of mass transfer characteristics using a tracer component.

Marangoni convection influences mass transfer as it stirs the phases and enhances the convective transport to and from the interface. The enhancement caused by convection is larger in the liquid phase than it is in the gas phase. However, for most systems that are suitable for studies on the influence of Marangoni convection, the resistance to mass transfer is located for a large part in the gas phase (an exception is the system diethyl ether-water-air [2, 4]). Decreasing the liquid side mass transfer resistance therefore increases the overall mass transfer rate much less than proportionally. For a better quantitative measurement of the increase of the liquid side mass transfer coefficient, a tracer component can be added [2, 3, 5]. This inert component is characterised by the following properties:

- The tracer component does not influence the surface tension.
- Mass transfer of the tracer component is limited by the liquid side mass transfer resistance only, due to the low solubility of the tracer in the liquid.
- The tracer component does not influence mass transfer of the component that affects the surface tension, nor does it react with any of the system components.
- The concentration of the tracer component should be relatively easy to measure.

Appropriate tracer components are inert gases, such as oxygen [3, 5], propene [2] and ethyne.

4.2 Description of the model

In a thin liquid film, microconvection is the main type of convection as usually no macroscopic concentration gradients parallel to the interface are present. Therefore, to get the best representation of mass transfer from a thin liquid film, only the convex container model of chapter 3 has been considered in this chapter. The model described in section 3.2 has been slightly adapted. The most important feature of the new model is the incorporation of a tracer component. As experimental studies have often tried to measure the enhancement of mass transfer by Marangoni convection by measuring the transfer of an inert component (see section 4.1), one additional convection-diffusion equation has been added to the set of equations described in chapter 3. This inert component has no influence on the surface tension, nor on any of the other variables already present in the model (such as viscosity, density, or diffusion coefficient). Therefore, there is no coupling between this additional convection-diffusion equation and the convection-diffusion equation of the surface tension lowering solute (from now on labelled simply ‘the solute’), the continuity equation or the Navier-Stokes equation.

The tracer component has been chosen to absorb into the liquid phase. All notation is equal to that in chapter 3. Dimensionless tracer concentration is denoted ζ. The boundary and initial conditions for ζ are:

$$\mathbf{n} \cdot \nabla \zeta = 0 \qquad \text{(left and right wall)} \qquad (23)$$

$$\zeta = 1 \qquad \text{(permeable top wall)} \qquad (24)$$

$$\zeta_{i,G} = \zeta_{i,L} \qquad \text{(interface)} \qquad (25)$$

$$\left.\frac{\partial \zeta}{\partial r}\right|_{L} = Bi_{N,\zeta} \left.\frac{\partial \zeta}{\partial r}\right|_{G} \qquad \text{(interface)} \qquad (26)$$

$$Bi_{N,\zeta} = m_{\zeta} \cdot \frac{D_{G,\zeta}}{D_{L,\zeta}} \qquad (27)$$

$$\zeta^{0}_{i,j} = 0 \qquad \forall\ i, j \le N_{wL+1} \qquad (28)$$

$$\zeta^{0}_{i,j} = 1 \qquad \forall\ i, j > N_{wL+1} \qquad (29)$$

Calculations were done with two different geometries. The gas phase was either chosen equally thick as the liquid phase ($H_G = H_L$), or a hundred times larger ($H_G = 100\ H_L$). In the latter geometry, diffusive mass transfer in the gas phase is allowed to proceed according to the penetration theory for the entire calculation time. In the former geometry, however, the mass transfer penetration depth exceeds the thickness of the gas phase shortly after the start of the calculation. The boundary condition at the permeable top wall ($c = 0$) then results in enhanced mass transfer in the gas phase. As a result, overall mass transfer rates are higher, and the Marangoni effect is expected to be stronger. The results of the computations showed, however, that calculations on both geometries yielded qualitatively the same results. Therefore, in this chapter, results are presented for one geometry only ($H_G = H_L$).

For the numerical model in chapter 3, a Biot number was introduced:

$$Bi_N = \frac{m\, D_G}{D_L} \qquad (30)$$

This Biot number is defined differently then the usual Biot number, and is therefore labelled the numerical Biot number. It should not be confused with the Biot number that is generally used to express the ratio of resistances to mass transfer in the liquid and the gas phase, Bi_R.

$$Bi_R = \frac{m\, k_G}{k_L} \qquad (31)$$

In this equation, k_G and k_L are the mass transfer coefficients on the liquid and the gas side, respectively. If mass transport in both phases proceeds according to the penetration theory, the Biot number can be written as:

$$Bi_R = m\sqrt{\frac{D_G}{D_L}} \qquad (32)$$

The real Biot number in the absence of convection can be calculated according to the following equation when the penetration depth in the gas phase is larger than H_G.

$$Bi_R = \frac{m}{Sc_G}\frac{H_L}{H_G}\sqrt{\pi\, t\, Sc_L} \qquad (33)$$

The latter equation is valid for most calculations in this chapter with small Marangoni numbers. The dimensionless interfacial concentrations can be calculated according to the following equation.

$$c_i = \left(\frac{1}{1+Bi_R}\right) \qquad (34)$$

In order to generalise the problem with respect to the problem posed in chapter 3, a non-zero initial gas phase concentration ($c_{G,0}$) is assumed. The problem which has to be solved remains the same when the governing equations are non-dimensionalised in the following way (the dimensionless concentrations are denoted by c; other concentrations are expressed in kg/m^3).

$$c = \frac{c_L - \frac{c_{G,0}}{m}}{c_{L,0} - \frac{c_{G,0}}{m}} \qquad \text{liquid phase} \qquad (35)$$

$$c = \frac{c_G - c_{G,0}}{m\,c_{L,0} - c_{G,0}} \qquad \text{gas phase} \qquad (36)$$

These definitions have no implications for the problem defined in chapter 3, other than that the Marangoni number is defined in a more general way.

$$Ma = \frac{\left(-\frac{\partial\gamma}{\partial c}\right)\left(c_{L,0} - \frac{c_{G,0}}{m}\right)H_L}{\mu D} \qquad (37)$$

The physical properties of the tracer component in this chapter have been set constant and equal to those of propene [2], i.e. $D_{L,\zeta}$ = 1.44 10^{-9} m^2/s, $D_{G,\zeta}$ = 1.22 10^{-5} m^2/s, m_ζ = 7.32 [kg/m^3 m^3/kg], $Bi_{N,\zeta}$ = 62017, $Sc_{L,\zeta}$ = 697.2, $Sc_{G,\zeta}$ = 1.266. Other parameter values, which do not change throughout this chapter either, are: μ_L = 1.002 10^{-3} Pa s, μ_G = 1.83 10^{-5} Pa s, ν_L = 1.004 10^{-6} m^2/s, ν_G = 1.5443 10^{-5} m^2/s, and $Vi_G = \nu_G/\nu_L$ = 15.38. One constant set of values has been used for the following numerical parameters introduced in chapter 3, pages 96-97: N_p = 2, N_θ = 60, N_{wL} = 60, N_{wG} = 31, ε = 0.05, X_{dist} = 0.0001, N_{dist} = 6.

Table 1. Values of parameters used in this chapter.

Case	D_G	D_L	m	Bi_N	Sc_G	Sc_L	Ma
	[m^2/s]	[m^2/s]	[-]	[-]	[-]	[-]	[-]
A1	1.04 10^{-5}	1.27 10^{-9}	1.6 10^{-4}	1.31	1.48	791	0
A2	1.04 10^{-5}	1.27 10^{-9}	1.6 10^{-4}	1.31	1.48	791	10^5

A3	$1.04\ 10^{-5}$	$1.27\ 10^{-9}$	$1.6\ 10^{-4}$	1.31	1.48	791	10^{6}
A4	$1.04\ 10^{-5}$	$1.27\ 10^{-9}$	$1.6\ 10^{-4}$	1.31	1.48	791	10^{7}
B1	$1.04\ 10^{-6}$	$1.27\ 10^{-9}$	$1.6\ 10^{-3}$	1.31	14.8	791	0
B2	$1.04\ 10^{-6}$	$1.27\ 10^{-9}$	$1.6\ 10^{-3}$	1.31	14.8	791	10^{5}
B3	$1.04\ 10^{-6}$	$1.27\ 10^{-9}$	$1.6\ 10^{-3}$	1.31	14.8	791	10^{6}
B4	$1.04\ 10^{-6}$	$1.27\ 10^{-9}$	$1.6\ 10^{-3}$	1.31	14.8	791	10^{7}
C1	$1.04\ 10^{-5}$	$1.27\ 10^{-8}$	$1.6\ 10^{-3}$	1.31	1.48	79.1	0
C2	$1.04\ 10^{-5}$	$1.27\ 10^{-8}$	$1.6\ 10^{-3}$	1.31	1.48	79.1	10^{4}
C3	$1.04\ 10^{-5}$	$1.27\ 10^{-8}$	$1.6\ 10^{-3}$	1.31	1.48	79.1	10^{5}
C4	$1.04\ 10^{-5}$	$1.27\ 10^{-8}$	$1.6\ 10^{-3}$	1.31	1.48	79.1	10^{6}
D1	$1.04\ 10^{-5}$	$1.27\ 10^{-9}$	$1.6\ 10^{-3}$	13.1	1.48	791	0
D2	$1.04\ 10^{-5}$	$1.27\ 10^{-9}$	$1.6\ 10^{-3}$	13.1	1.48	791	10^{5}
D3	$1.04\ 10^{-5}$	$1.27\ 10^{-9}$	$1.6\ 10^{-3}$	13.1	1.48	791	10^{6}
D4	$1.04\ 10^{-5}$	$1.27\ 10^{-9}$	$1.6\ 10^{-3}$	13.1	1.48	791	10^{7}
D5	$1.04\ 10^{-5}$	$1.27\ 10^{-9}$	$1.6\ 10^{-3}$	13.1	1.48	791	10^{4}
E1	$1.04\ 10^{-5}$	$1.27\ 10^{-9}$	$1.6\ 10^{-2}$	131	1.48	791	0
E2	$1.04\ 10^{-5}$	$1.27\ 10^{-9}$	$1.6\ 10^{-2}$	131	1.48	791	10^{5}
E3	$1.04\ 10^{-5}$	$1.27\ 10^{-9}$	$1.6\ 10^{-2}$	131	1.48	791	10^{6}
E4	$1.04\ 10^{-5}$	$1.27\ 10^{-9}$	$1.6\ 10^{-2}$	131	1.48	791	10^{7}
F1	$1.04\ 10^{-4}$	$1.27\ 10^{-9}$	$1.6\ 10^{-3}$	131	0.148	791	0
F2	$1.04\ 10^{-4}$	$1.27\ 10^{-9}$	$1.6\ 10^{-3}$	131	0.148	791	10^{5}
F3	$1.04\ 10^{-4}$	$1.27\ 10^{-9}$	$1.6\ 10^{-3}$	131	0.148	791	10^{6}
F4	$1.04\ 10^{-4}$	$1.27\ 10^{-9}$	$1.6\ 10^{-3}$	131	0.148	791	10^{7}
G1	$1.04\ 10^{-5}$	$1.27\ 10^{-10}$	$1.6\ 10^{-3}$	131	1.48	7910	0
G2	$1.04\ 10^{-5}$	$1.27\ 10^{-10}$	$1.6\ 10^{-3}$	131	1.48	7910	10^{6}
G3	$1.04\ 10^{-5}$	$1.27\ 10^{-10}$	$1.6\ 10^{-3}$	131	1.48	7910	10^{7}
G4	$1.04\ 10^{-5}$	$1.27\ 10^{-10}$	$1.6\ 10^{-3}$	131	1.48	7910	10^{8}

The grid refinement parameters a and b (see page 96) have been set to a value of 0.5. Initial conditions were obtained by calculating for 100 time steps with $\Delta t = 5\ 10^{-5}$ (dimensionless) and Ma = 0. For the calculation itself $\Delta t = 5\ 10^{-4}$ and $N_t = 4000$.

For this chapter, calculations have been done with varying Marangoni numbers (as defined in equation (37)), solute liquid and gas phase diffusivities, and solute distribution coefficients. Results are primarily presented in graphs depicting the dimensionless solute or tracer mass in the liquid phase as a function of time. The mass in the container was calculated

each time step by numerically integrating the dimensionless concentration over the total liquid phase area. Other graphs present the maximum interface velocity as a function of time, and the solute interface concentration as a function of the position along the interface at a particular point in time. The maximum interface velocity was calculated after each one tenth of the total calculation time, i.e. after 400 time steps.

In table 1, the parameter values are shown, which have been used for the calculations presented in this chapter. It is important to understand the differences between the various cases in order to comprehend the presentation and the discussion of the results. The base case used for the computations is case D. The values for the gas and the liquid phase diffusivity, and the distribution coefficient in the base case correspond to the properties of the acetone-water system described in chapter 3. For the base case, the properties of the solute are: $D_L = 1.27\ 10^{-9}$ m^2/s, $D_G = 1.04\ 10^{-5}$ m^2/s, $m = 1.60\ 10^{-3}$ [kg/m^3 m^3/kg], i.e. $Bi_N = 13.1$, $Sc_L = 791$, and $Sc_G = 1.48$. Calculations for six other cases (A, B, C, E, F, G) have been performed. In each of these cases, one of the parameters D_L, D_G, or m is either ten times larger or ten times smaller than in the base case (see table 1). For each of these seven cases, calculations with four different values of the Marangoni number have been performed. Only in the base case, calculations with five different values of the Marangoni number have been performed. The numbers in each of the cases correspond. For example, for each of the cases A4-B4-C4-D4-E4-F4-G4 the ratio Ma/Sc_L is equal. Summarising, the letters (A-G) refer to a particular combination of D_L, D_G, m (or Sc_L, Sc_G, Bi_N), and the numbers (1-5) refer to a particular ratio Ma/Sc_L.

In the following three sections, results of the calculations are presented. In section 4.6, a comparison is made between literature results listed in section 4.1 and the results presented in sections 4.3-4.5. In section 4.6 also an attempt is made to verify equations (1) and (2), and determine a value for n.

Results are presented in dimensionless form. Recall from chapter 3 that distance, time, stream function, and vorticity have been non-dimensionalised by scaling with H_L, H_L^2/ν_L, ν_L, and ν_L/H_L^2, respectively. Note that no absolute value for H_L has been chosen for the calculations in this chapter, and that the results are valid for any value of H_L. Remember, however, that the parameter H_L features in the Marangoni number. That is, when all other parameters in the Marangoni number are equal, results for a layer of 1 cm and $Ma = 10^7$ should be compared to results in a layer of 1 mm and $Ma = 10^6$.

4.3 Influence of distribution coefficient

Apart from the base case ($m = 1.60\ 10^{-3}$), calculations have been done for values of the distribution coefficient which are ten times larger than, and ten times smaller than that of the base case, resulting in various values of the numerical Biot number, $Bi_N = 1.31$ (case A), $Bi_N = 13.1$ (case D), and $Bi_N = 131$ (case E). See table 1 for all parameter values.

In figure 3, the integrated dimensionless mass of the solute in the liquid phase is presented as a function of time for various values of Bi_N and Ma. Note that the integrated mass at $t = 0$ approximately equals $\pi/4$ due to the shape of the liquid phase.

From figure 3 several conclusions can be drawn. For $Bi_N = 13.1$ and $Ma = 10^5$, the Marangoni effect starts to accelerate the mass transfer only after $t = 0.9$. For the other

numerical Biot numbers, no influence on the mass transfer can be observed for $Ma = 10^5$. For $Ma = 10^6$ and $Ma = 10^7$, the mass transfer is increased by the Marangoni effect for all numerical Biot numbers. At first impression, the effect is the largest for $Bi_N = 131$. However, since for $Bi_N = 131$ the resistance to mass transfer is located in the liquid phase, an increase in the liquid side mass transfer coefficient has the most notable influence on the total mass transfer. In order to see only the influence on the liquid side mass transfer coefficient, it is better to study the mass transfer of the tracer component, which is limited by the liquid side mass transfer resistance only. In figure 4, the integrated mass of tracer in the liquid phase is presented as a function of time.

From figure 4, it can be concluded that the liquid side mass transfer coefficient is enhanced most for $Bi_N = 13.1$, and least for $Bi_N = 1.31$. However, the enhancement is comparable for all numerical Biot numbers. In figure 5, the maximum interface velocity as a function of time, Biot, and Marangoni number is presented. As one expects, the trend for the dependence of the liquid side mass transfer coefficient on the numerical Biot number is similar to the trend for the dependence of the maximum interface velocity on the numerical Biot number. It can be observed that the interface velocities for $Ma = 10^5$ grow exponentially in time. It is therefore reasonable to assume, that also for $Bi_N = 1.31$ and $Bi_N = 131$, enhancement of mass transfer will be observed after some critical time. This concept of a critical time was already established by Brian and Ross [11], and Dijkstra [12], among other authors. The growth factor of the interfacial velocities, and therefore the critical time, is dependent on the difference between the actual Marangoni number and the critical Marangoni number. Initial growth factors and the critical Marangoni number could in principal be calculated using a linear stability analysis [13].

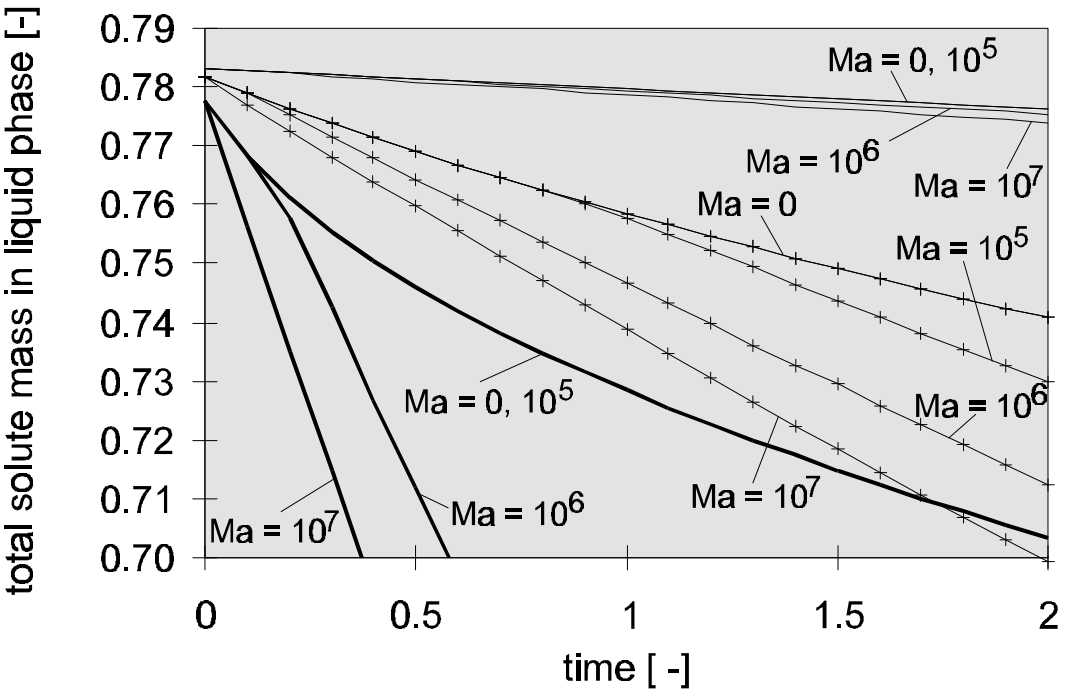

figure 3 *Total solute mass in liquid phase as a function of time for various distribution coefficients and Marangoni numbers. Schmidt numbers equal those of the base case (case D). Legend: —— $m = 1.6\ 10^{-4}$ (case A); —+— $m = 1.6\ 10^{-3}$ (case D); ——— $m = 1.6\ 10^{-2}$ (case E)*

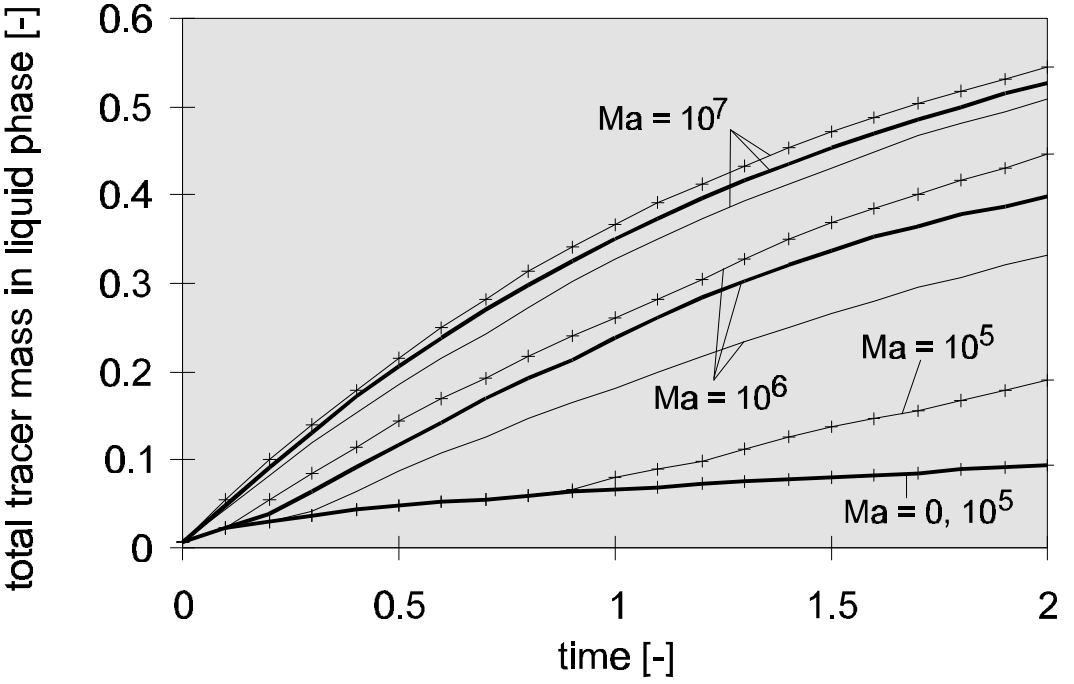

figure 4 *Total tracer mass in liquid phase as a function of time for various solute distribution coefficients and Marangoni numbers. Schmidt numbers equal those of the base case (case D).*
Legend: —— $m = 1.6\ 10^{-4}$ (case A); —+— $m = 1.6\ 10^{-3}$ (case D); ——— $m = 1.6\ 10^{-2}$ (case E)

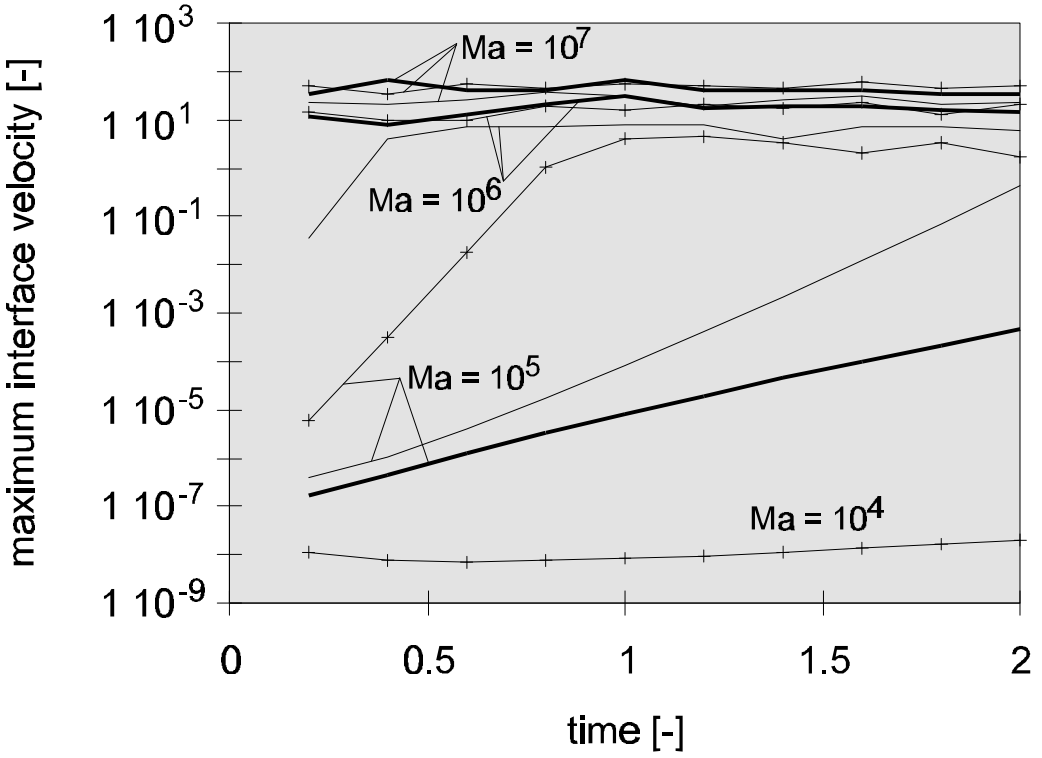

figure 5 *Maximum interface velocity as a function of time for various distribution coefficients and Marangoni numbers. Schmidt numbers equal those of the base case (case D).*
Legend: —— *m = 1.6 10^{-4} (case A);* —+— *Bi_N = m = 1.6 10^{-3} (case D);* ━━ *m = 1.6 10^{-2} (case E)*

To explain why the enhancement of mass transfer is largest for Bi_N = 13.1, it is instructive to have a look at the interfacial solute concentrations for the three cases as well. Interfacial concentration profiles at t = 2 are presented in figure 6. From this figure, it is clear that the curves corresponding to Bi_N = 13.1 and Ma = 0 are closest to 0.5. That is, for Bi_N = 13.1, the resistances in the gas phase and the liquid phase are approximately equal (see the formula for the interfacial concentration (34)). For Bi_N = 1.31, most resistance to mass transfer is in the gas phase, and for Bi_N = 131 most resistance is in the liquid phase. The Marangoni effect is largest when the concentration gradients parallel to the interface are largest. When the mass transfer resistance is located mainly in one of the phases, mass transfer in the other phase levels out the concentration gradients parallel to the interface. Approximately equal mass transfer resistances (Bi_R close to 1; c_i close to 0.5) therefore yield the largest Marangoni effect.

The results, however, do point out that additional factors play a role. For example, for Bi_N = 13.1 and Ma = 10^7 (case D4), c_i at t = 2 equals 0.8, while for Bi_N = 131 and Ma = 10^7 (case E4), c_i at t = 2 equals 0.27. According to the hypothesis stated above, the liquid side mass transfer coefficient (and the maximum interface velocity) should therefore be larger for Bi_N = 131 (0.27 being closer to 0.5 than 0.8), but figures 4 and 5 indicate that this not the case. In section 4.6, these results are discussed in some more detail.

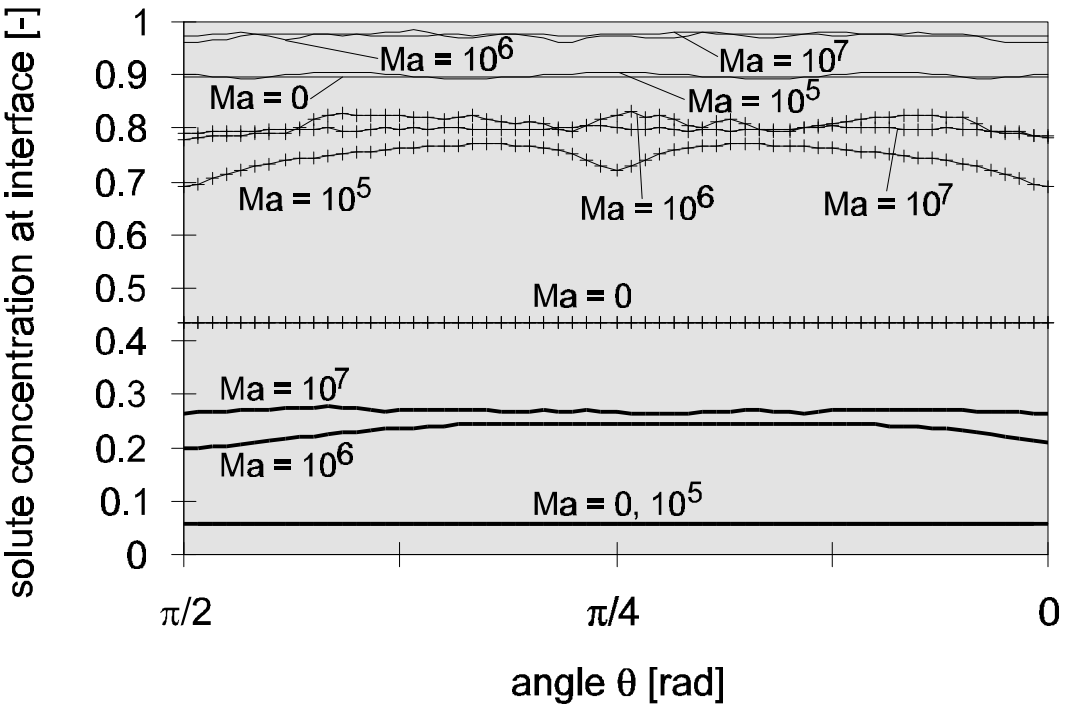

figure 6 *Interfacial concentration at t = 2 for various distribution coefficients and Marangoni numbers. Schmidt numbers equal those of the base case (case D). Legend: ── m = 1.6 10^{-4} (case A); ─┼─ m = 1.6 10^{-3} (case D); ━━ m = 1.6 10^{-2} (case E)*

The development of concentration and flow patterns is qualitatively similar for all three cases, and conclusions can be drawn along the same lines as in chapter 3. Initially, patterns form with varying numbers of roll cells. Relatively soon, a four roll cell pattern is established, which finally turns into a two roll cell pattern. The larger the Marangoni number, the faster the transitions to the four roll cell pattern and then to the two roll cell pattern occur. Especially for larger Marangoni numbers, small roll cells superposed on the basic two roll cell pattern grow and disappear, and sometimes a four roll cell pattern reoccurs temporarily. After a short initial period, the roll cells closest to the solid walls always turns in such a way that the flow along the gas-liquid interface is directed towards the solid boundary. In figure 7, concentration fields and flow patterns are presented for four different cases. Some calculations which are not listed in table 1 have been pursued for a longer dimensionless time, and these calculations show that concentration and flow patterns become smoother when solute is depleted from the V-shaped container. Figure 8 outlines results for two such cases for which H_G = 100 H_L. For the presentation of the results in these figures, the same convention is adopted as in chapter 3 (page 103).

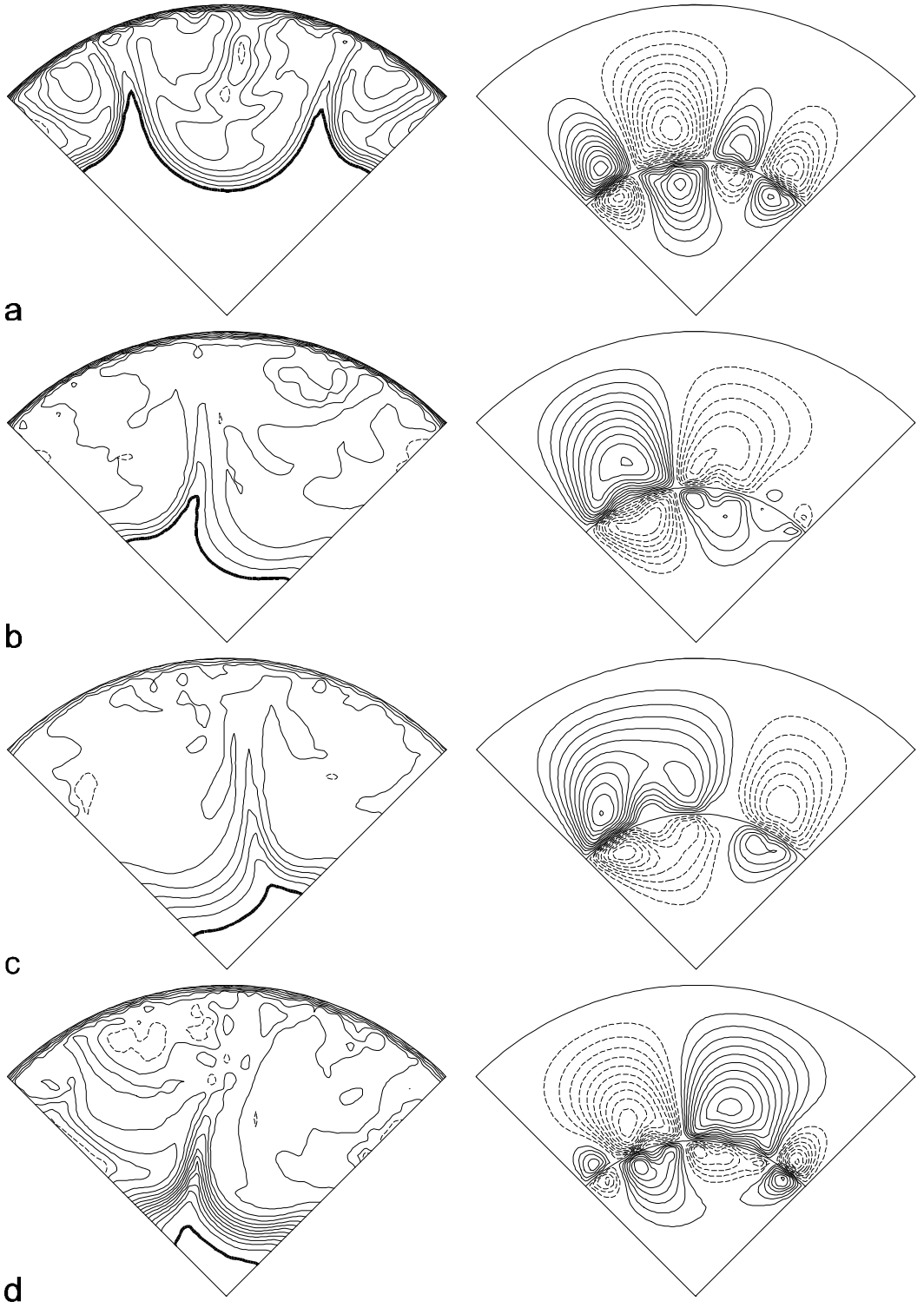

figure ***Fout! Bladwijzer niet gedefinieerd.*** *Liquid phase concentration field (left) and full geometry flowpattern (right) at t = 2; a. case A3, C_{max} = 0.9975, D_C = 0.0025, D_S = 0.02, b. case A4, C_{max} = 0.9975, D_C = 0.0025, D_S = 0.1; c. case D4, C_{max} = 0.99, D_C = 0.02, D_S = 0.2; d. case E4, C_{max} = 0.99, D_C = 0.04, D_S = 0.1*

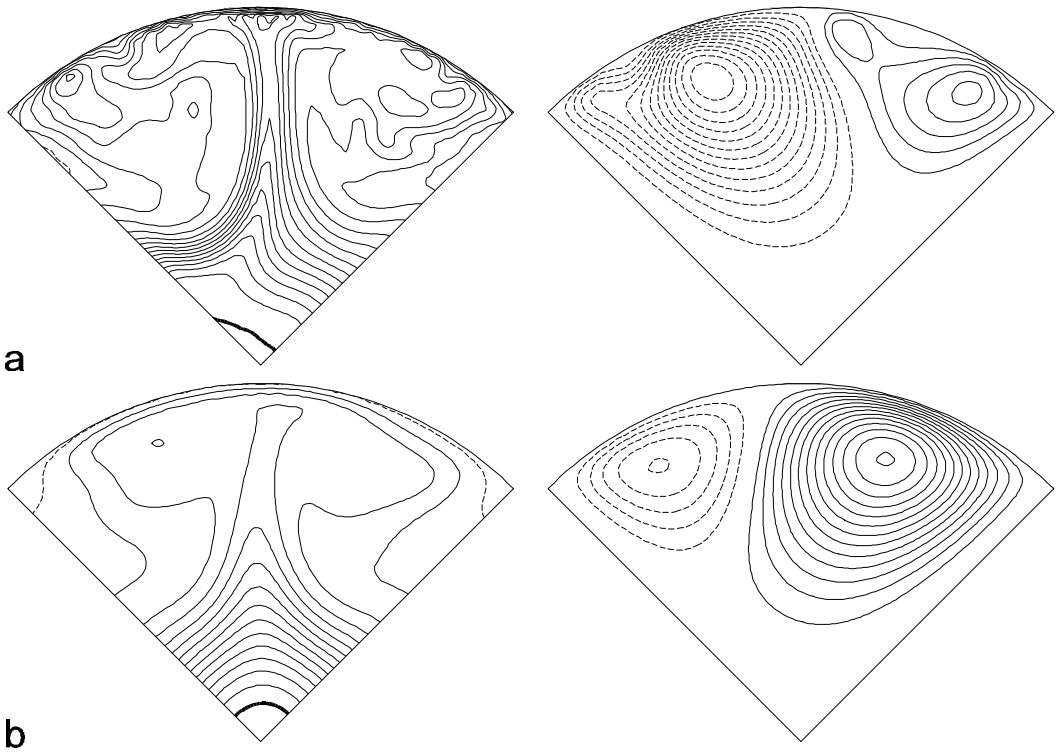

figure 8 *Evolution of liquid phase concentration field (left) and liquid phase flowpattern (right) (H_G = 100 H_L); Bi_N = 131, Sc_L = 791, Sc_G = 1.48, Ma = 5 10^5, a. At t = 4; C_{max} = 0.99, D_C = 0.04, D_S = 0.04; b. At t = 40; C_{max} = 0.34, D_C = 0.02, D_S = 0.004.*

In figures **Fout! Bladwijzer niet gedefinieerd.**a and **Fout! Bladwijzer niet gedefinieerd.**b, an example can be observed of the general trend that the transition time from a four roll cell pattern to a two roll cell pattern occurs at a later time for a smaller Marangoni number. Figures **Fout! Bladwijzer niet gedefinieerd.**b-**Fout! Bladwijzer niet gedefinieerd.**d compare patterns obtained with different numerical Biot numbers. The patterns are qualitatively similar, although absolute concentration gradients differ considerably, reflecting the different Biot numbers. Finally, figure 8 presents results for a different geometry (H_G = 100 H_L). The figure shows that concentration and flow patterns become smoother in time, as the solute is depleted from the liquid.

4.4 Influence of gas phase diffusion coefficient

Apart from the base case (D_G = 1.04 10^{-5} m^2/s), calculations have been done for values of the gas phase diffusivity which are ten times larger than, and ten times smaller than that of the base case, resulting in various values of the solute numerical Biot number Bi_N and the solute gas phase Schmidt number Sc_G, i.e. Bi_N = 1.31, Sc_G = 14.8 (case B); Bi_N = 13.1 and Sc_G = 1.48 (case D); Bi_N = 131 and Sc_G = 0.148 (case F). See table 1 for all parameter values.

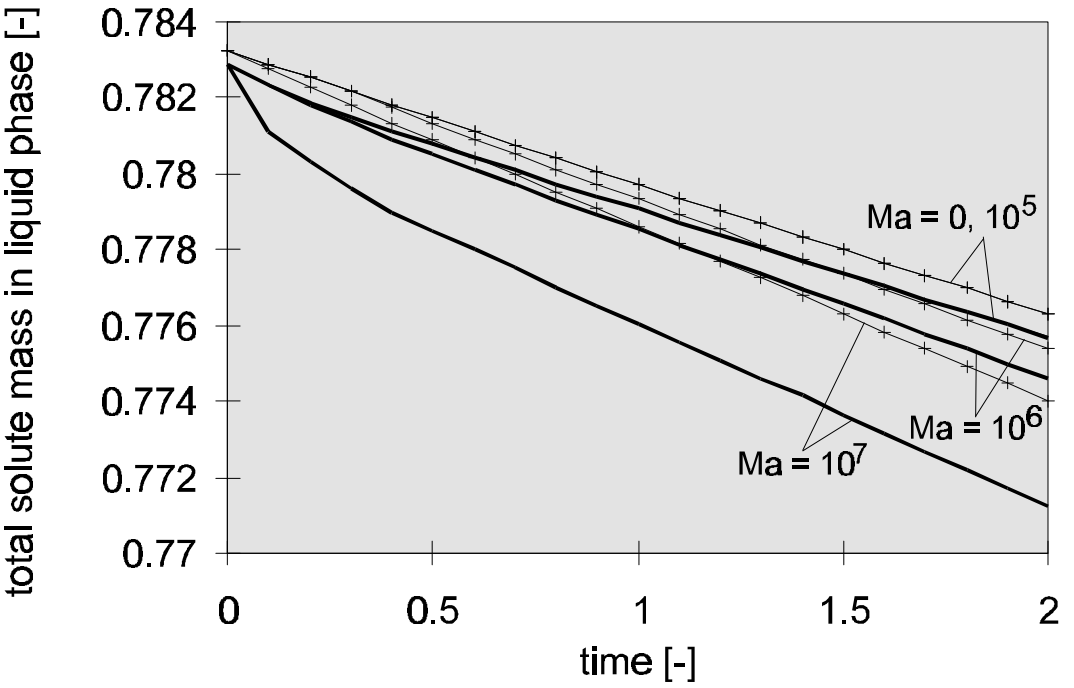

figure 9 *Total solute mass in liquid phase as a function of time for various gas phase diffusivities, distribution coefficients and Marangoni numbers. Sc_L = 791 and Bi_N = 1.31 for all cases.*
Legend: —+— Sc_G = 1.48 (case A); —— Sc_G = 14.8 (case B)

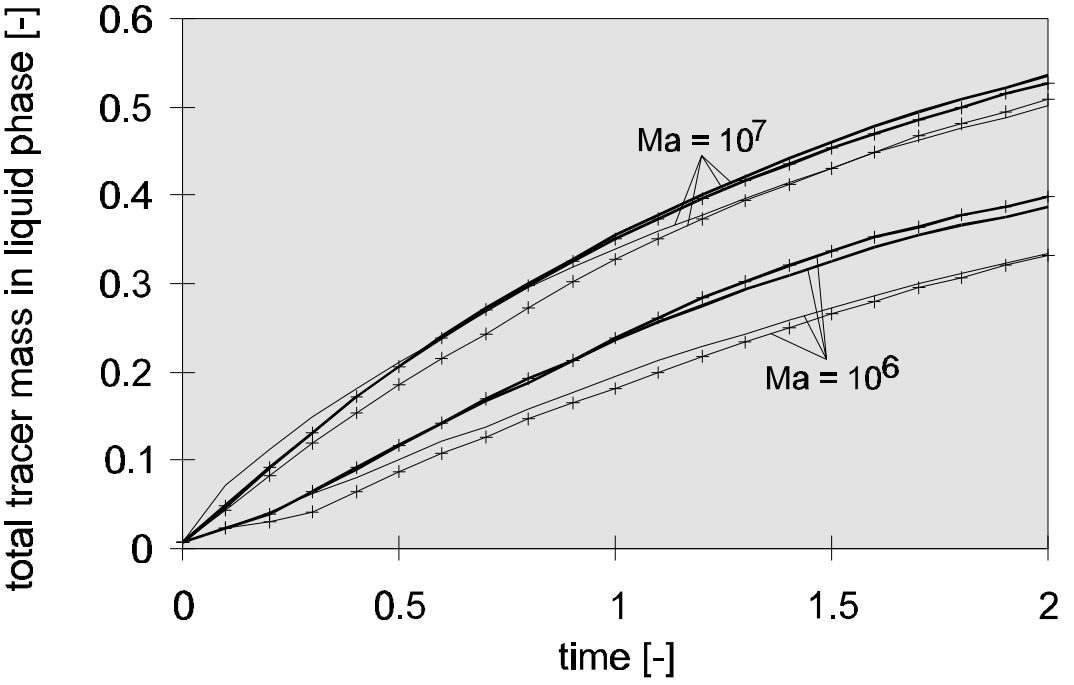

figure 10 *Total tracer mass in liquid phase as a function of time for various gas phase diffusivities, distribution coefficients and Marangoni numbers. Sc_L = 791 for all cases. Legend: —+— Bi_N = 1.31, Sc_G = 1.48 (case A); —+— Bi_N = 131, Sc_G = 1.48 (case E); —— Bi_N = 1.31, Sc_G = 14.8 (case B); —— Bi_N = 131, Sc_G = 14.8 (case F).*

The discussion in this section is focused on the comparison between the results in this section and those of the last section. I.e., results are compared between cases with equal Bi_N, but different gas phase diffusivities. In figure 9, the integrated dimensionless mass of the solute in the liquid phase is presented for cases A and B, for various Marangoni numbers. In figure 10, the integrated dimensionless tracer mass in the liquid phase is presented for cases A and B, E and F, and Ma = 10^6 and 10^7.

Figure 10 shows that for equal Marangoni numbers the two curves for cases E and F are almost identical, but from figures 9 and 10, it is also apparent that for equal Marangoni number, the curves for cases A and B are somewhat further apart. For Ma = 10^7 and Sc_G = 14.8 (case B4), there is a steep enhancement of mass transfer between t = 0 and t = 0.2, both manifest in figures 9 and 10. For larger t, the enhancement of the liquid phase mass transfer coefficient diminishes and becomes smaller than the enhancement of mass transfer for case A4 (figure 10). The enhancement of the total mass transfer coefficient for case B4 remains higher than that of case A4 for the entire calculation time (figure 9).

The initially very steep enhancement of mass transfer for case B4 is even large compared to the enhancement of mass transfer for the case D4 (Bi_N = 13.1), although the interfacial concentration of the latter case is closer to 0.5 (also for small t). This phenomenon can be explained by the small absolute value of the gas phase diffusion coefficient. The dimensionless penetration depth in a phase P (δ_P) is given by the following equation:

$$\delta_P = \sqrt{\frac{\pi t}{Sc_P}} \qquad (38)$$

For case B and t = 0.1, δ_G = 0.6, i.e. the penetration depth is smaller than the gas phase film thickness. For these small times, the gradient of concentration in the gas phase is therefore higher for case B than for all other cases. Bi_R for case B is consequently larger and the interfacial concentration is smaller, i.e. closer to 0.5, than for case A. This analysis explains why initially the enhancement of mass transfer is higher for case B than for case A. An explanation for the fact that the enhancement of mass transfer is initially also higher for case B than for case D is also based on the small absolute value of the gas phase diffusion coefficient. Apart from the larger gradients at the interface associated with the smaller diffusivity, the small diffusivity in the gas phase also renders the initial characteristic roll cell size smaller, and the number of roll cells larger. Therefore, mass transfer is enhanced along the entire interface. In figure 11, initial roll cell patterns for case B, D, and F are compared.

One could suspect that during the small initial period during which the mass transfer is enhanced abnormally, the interface is occupied with what Golovin labels chaotic roll cells (type A). In this period the enhancement of mass transfer is proportional to Ma, rather than to $Ma^{1/3}$ (see introduction). In gas-liquid systems the transition from chaotic roll cells to structured roll cells usually occurs fast, due to the large gas phase diffusion coefficient. In liquid-liquid systems the diffusion coefficient in the second phase is small, and that is probably why Golovin mostly finds linear k_L - Ma relationships for liquid-liquid systems.

Finally, an explanation needs to be found for the fact that solute liquid side mass transfer for case B is more enhanced than for case A for small time, but not for larger time (figure 10),

while overall solute mass transfer for case B is more enhanced than for case A for the entire calculation time (figure 9). Again the small diffusivity of the solute in case B provides an explanation. Convection in the gas phase contributes more to the overall mass transfer process in case B and enhances the gas phase mass transfer, while in case A the transport by convection is smaller than the transport by diffusion. The ratio of convective and diffusive mass transfer is expressed in the Peclet number.

$$\mathrm{Pe} = \left(\frac{\mathrm{d}\psi}{\mathrm{dx}} \right) \mathrm{Sc}_{\mathrm{G}} \qquad (39)$$

At t = 2, Pe = 0.3 for case A4, and Pe = 1.5 for case B4, when a value of dψ/dx (vertical velocity) is estimated at the middle of the container. These values of Pe represent upper values, as velocities are generally smaller. From the value of Pe for B4, one can see that convective mass transport for this case does contribute to the mass transfer in the gas phase.

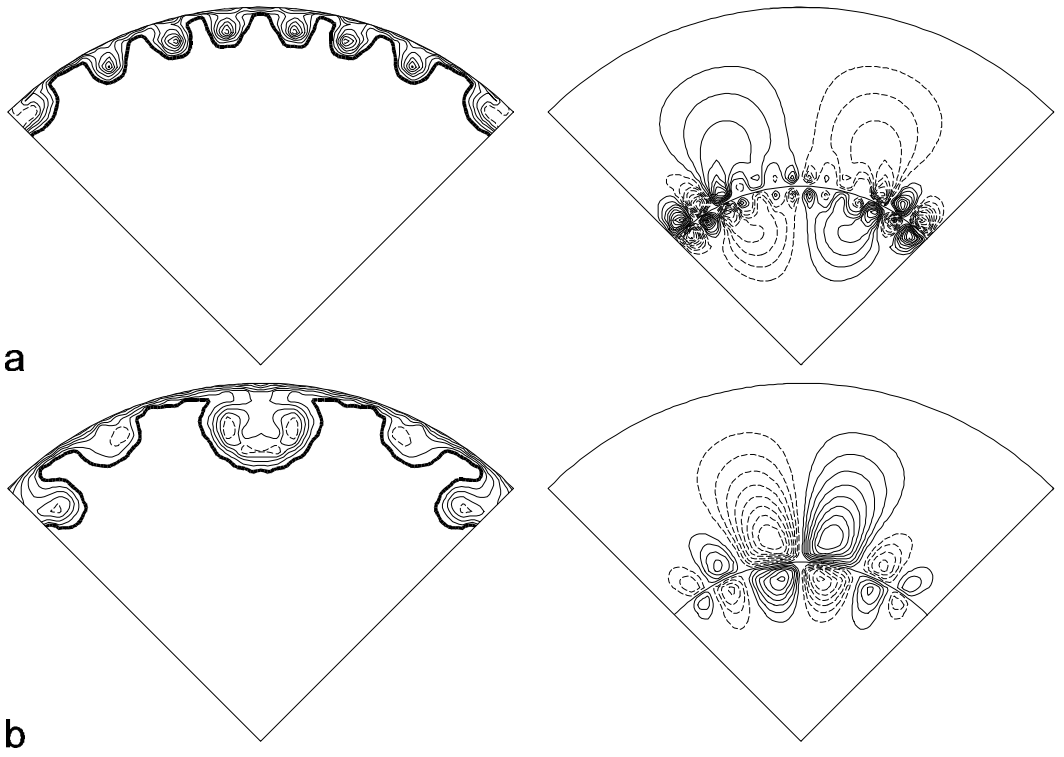

figure 11 Liquid phase concentration field (left) and full geometry flowpattern (right) at t = 0.2; a. Case B3, C_{max} = 0.9975, D_C = 0.005, D_S = 0.005; b. Case D3, C_{max} = 0.99, D_C = 0.02, D_S = 0.05.

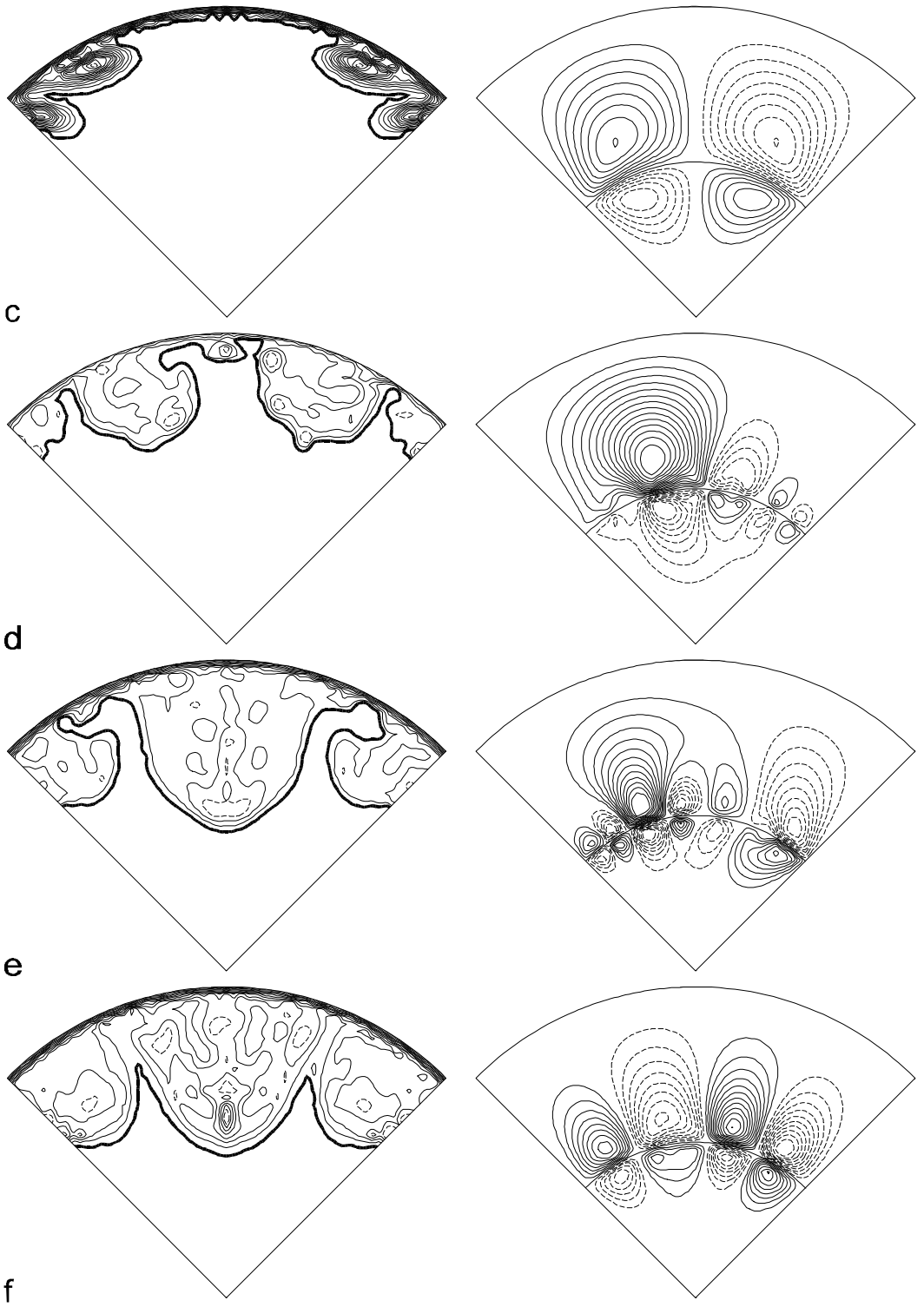

figure 11 *c. Case F3, C_{max} = 0.99, D_C = 0.04, D_S = 0.2; d. Case B4, C_{max} = 0.9975, D_C = 0.005, D_S = 0.05; e. Case D4, C_{max} = 0.99, D_C = 0.02, D_S = 0.1; f. Case F4; C_{max} = 0.99, D_C = 0.04, D_S = 0.2*

4.5 Influence of liquid phase diffusion coefficient

Apart from the base case (D_L = 1.27 10^{-9} m^2/s), calculations have been done for values of the solute liquid phase diffusivity which are ten times larger than, and ten times smaller than that of the base case, resulting in various values of the solute numerical Biot number Bi_N and the solute liquid phase Schmidt number Sc_L, i.e. Bi_N = 1.31, Sc_L = 79.1 (case C); Bi_N = 13.1 and Sc_L = 791 (case D); Bi_N = 131 and Sc_L = 7910 (case G). See table 1 for all parameter values. Note that the liquid phase diffusion coefficient features in the Marangoni number as well. Therefore, in order to make a comparison between cases C, D and G, the Marangoni numbers are not the same in these cases. For example, for case C4 Ma = 10^6, for case D4 Ma = 10^7, and for case G4 Ma = 10^8 (see table 1). In some of the figures, therefore, results are discriminated with a case number (e.g. 'case 4'), rather than with the Marangoni number.

Results for the solute and tracer hold-up in the liquid phase and the maximum interface velocity as a function of time are presented in figures 12, 13 and 14, respectively.

In figure 12, similar trends can be observed as in figure 3. Enhancement of overall mass transfer by Marangoni convection is relatively largest for the case with the largest Biot number (case G). Figure 13 demonstrates that again the largest enhancement of liquid side mass transfer is obtained for the case with the intermediate Biot number (Bi_N = 13.1; case D). The smallest enhancement of liquid side mass transfer is obtained for the case with the largest Biot number (Bi_N = 131; case G). These results compare qualitatively to the results for the maximum interface velocities presented in figure 14. In order to check whether these results can be explained with the values of the real Biot number, interfacial concentrations at t = 2 are plotted for cases C, D, and G in figure 15. Again, the theory that the real Biot number should be 1 (interfacial concentration = 0.5) to obtain the largest Marangoni effect is not exact. For cases C2-D2-G2, C3-D3-G3, and C4-D4-G4, the interfacial concentration for Bi_N = 131 (G) is closest to 0.5, and for Bi_N = 1.31 (C) furthest away. Nevertheless, case D brings about the largest enhancement of liquid side mass transfer, and case G the smallest. As in section 4.3, it has to be concluded that also another parameter than the real Biot number plays a significant role. In order to understand some of the effects discussed above more quantitatively, a semi-quantitative model is developed in section 4.6.

Concentration and flow patterns at t = 2 for the cases C4 and G4 are presented in figure 16. It can clearly be seen that the large value of the liquid diffusivity in case C smoothes out concentration gradients in the liquid phase. This also leads to a regular flow pattern, and, despite the larger velocities in case C, no small rolls develop superposed on the two large roll cells in case C4.

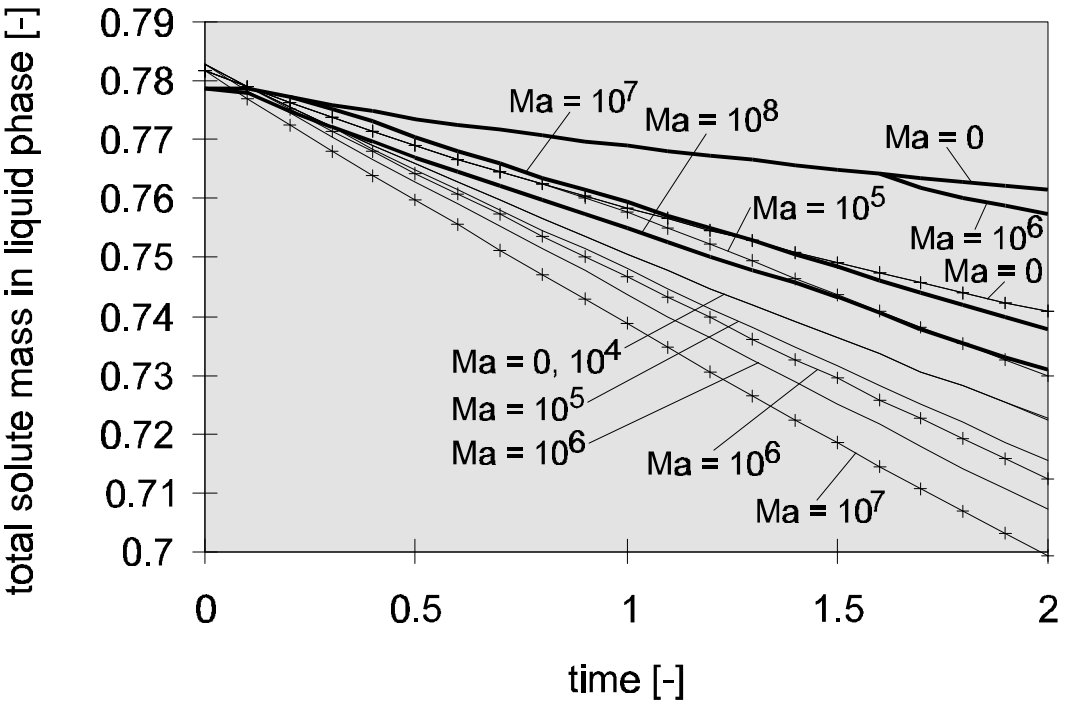

figure 12 *Total solute mass in liquid phase as a function of time for various solute liquid phase diffusivities and Marangoni numbers. Sc_G = 1.48 for all cases. Legend: —— D_L = 1.27 10^{-8} m^2/s (case C); —+— D_L = 1.27 10^{-9} m^2/s (case D); ▬▬ D_L = 1.27 10^{-10} m^2/s (case G)*

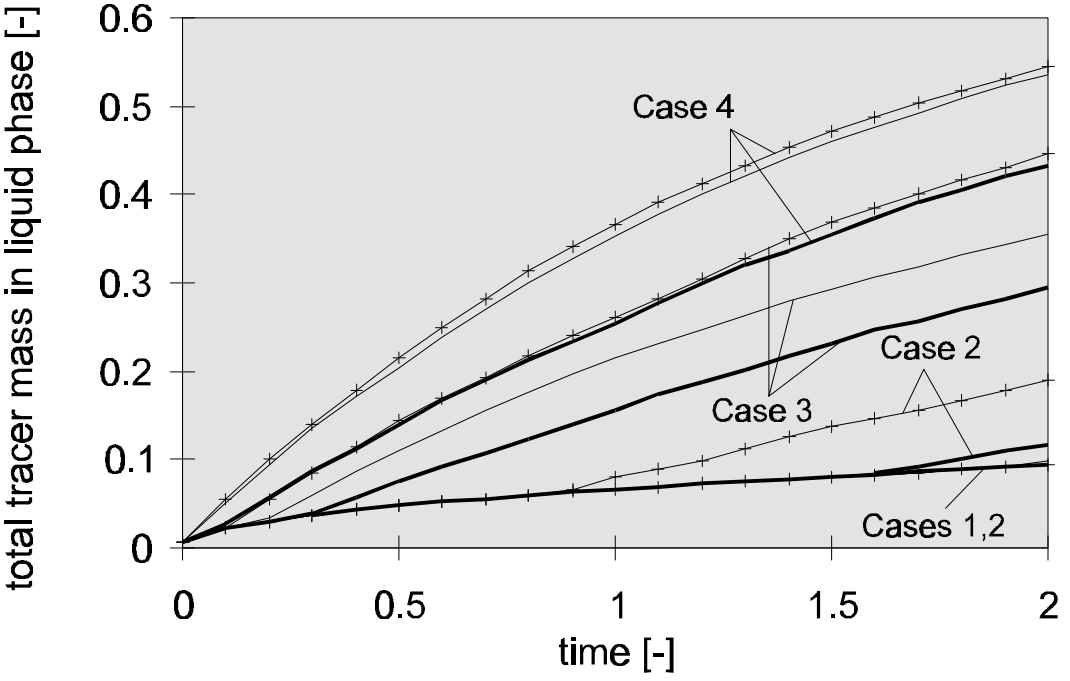

figure 13 *Total tracer mass in liquid phase as a function of time for various solute liquid phase diffusivities and Marangoni numbers. Sc_G = 1.48 for all cases. Legend: —— D_L = 1.27 10^{-8} m^2/s (case C); —+— D_L = 1.27 10^{-9} m^2/s (case D); ▬▬ D_L = 1.27 10^{-10} m^2/s (case G)*

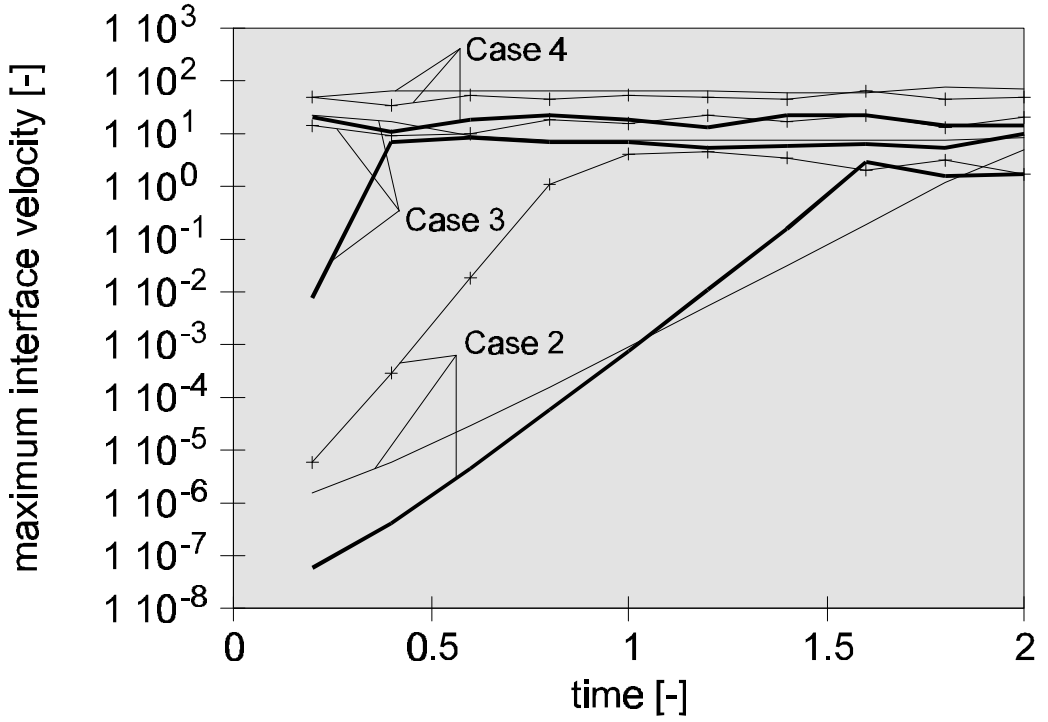

figure 14 *Maximum interface velocity as a function of time for various solute liquid phase diffusivities. Sc_G = 1.48 for all cases.*
Legend: —— D_L = 1.27 10^{-8} m^2/s (case C); —+— D_L = 1.27 10^{-9} m^2/s (case D); ━━ D_L = 1.27 10^{-10} m^2/s (case G)

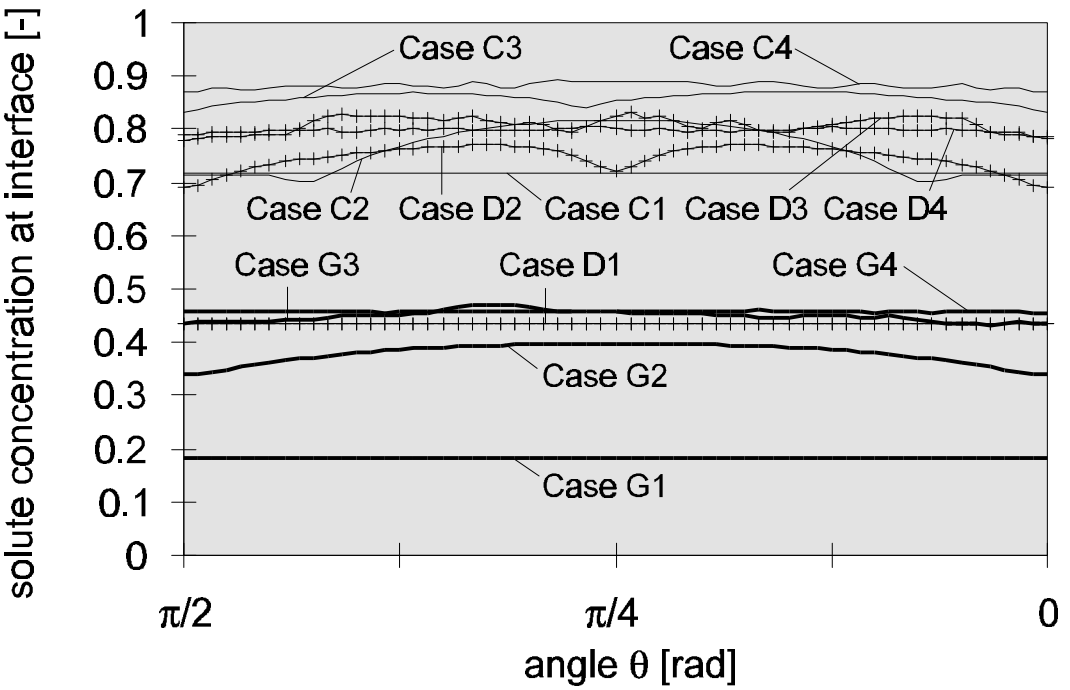

figure 15 *Interfacial concentration at t = 2 for various solute liquid phase diffusion coefficients. Sc_G = 1.48 for all cases.*
Legend: —— D_L = 1.27 10^{-8} m^2/s (case C); —+— D_L = 1.27 10^{-9} m^2/s (case D); ━━ D_L = 1.27 10^{-10} m^2/s (case G)

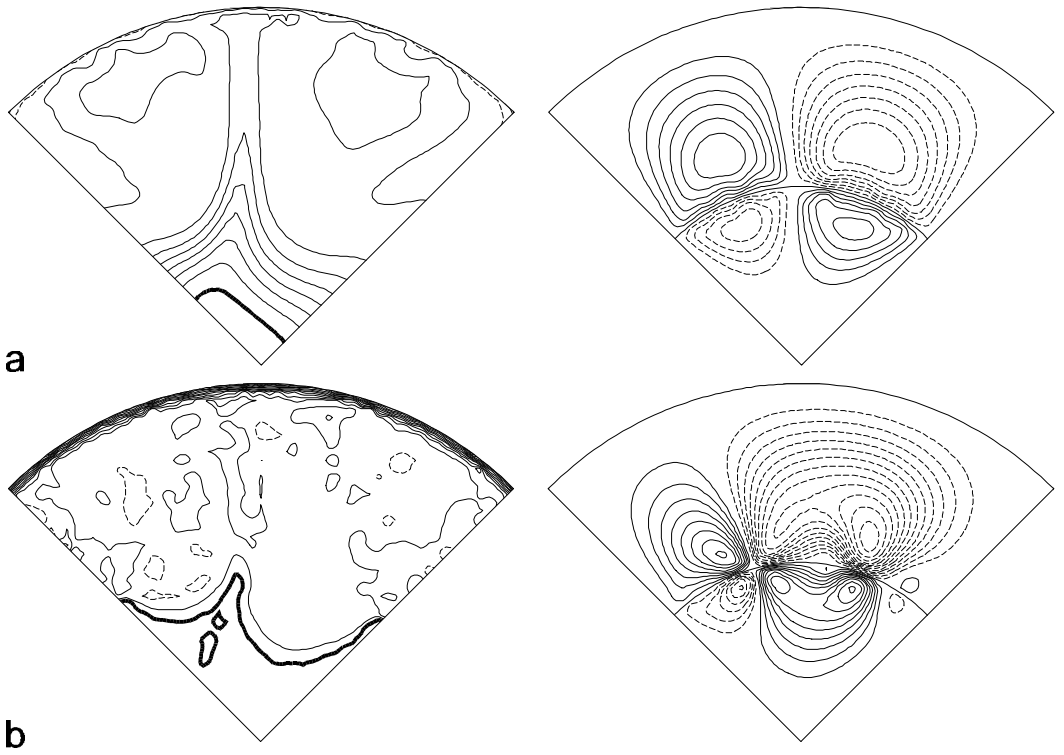

figure 16 Liquid phase concentration field (left) and full geometry flowpattern (right) at t = 2; a. Case C4, C_{max} = 0.96, D_C = 0.01, D_S = 0.4; b. Case G4, C_{max} = 0.99, D_C = 0.04, D_S = 0.05

4.6 Discussion and comparison with literature

Influence of the real Biot number

The results presented in sections 4.3-4.5 indicate that the largest enhancement of liquid side mass transfer is obtained for cases with intermediate (real) Biot numbers. Results for tracer hold-up as a function of time for the cases A3-G3 and A4-G4 are summarised in figure 17. In order to interpret this rather busy graph, recall that for all cases A3-G3 the dependence of surface tension on concentration is equal, and that the same applies for all cases A4-G4 (see table 1). In both series of curves A3-G3 and A4-G4, case D shows the largest enhancement of mass transfer. Case G leads to the smallest enhancement of mass transfer by the Marangoni effect.

The largest enhancement of mass transfer occurs when the velocities are largest, which occurs when the surface tension gradients are largest, which in turn occurs when the concentration gradients parallel to the interface are largest. The following discussion is focused on providing a qualitative explanation for the result that the largest enhancement of mass transfer, implying the largest concentration gradient parallel to the interface, is found for intermediate Biot numbers.

Two analyses are presented. Firstly, an explanation is given for the fact that for small Marangoni number, the growth of the maximum velocity with time is largest for intermediate real Biot numbers. Then, a similar explanation is presented for why enhancement of mass transfer is the largest for the cases with intermediate real Biot numbers when convection is the main mass transfer mechanism in the liquid phase (i.e. large Marangoni number).

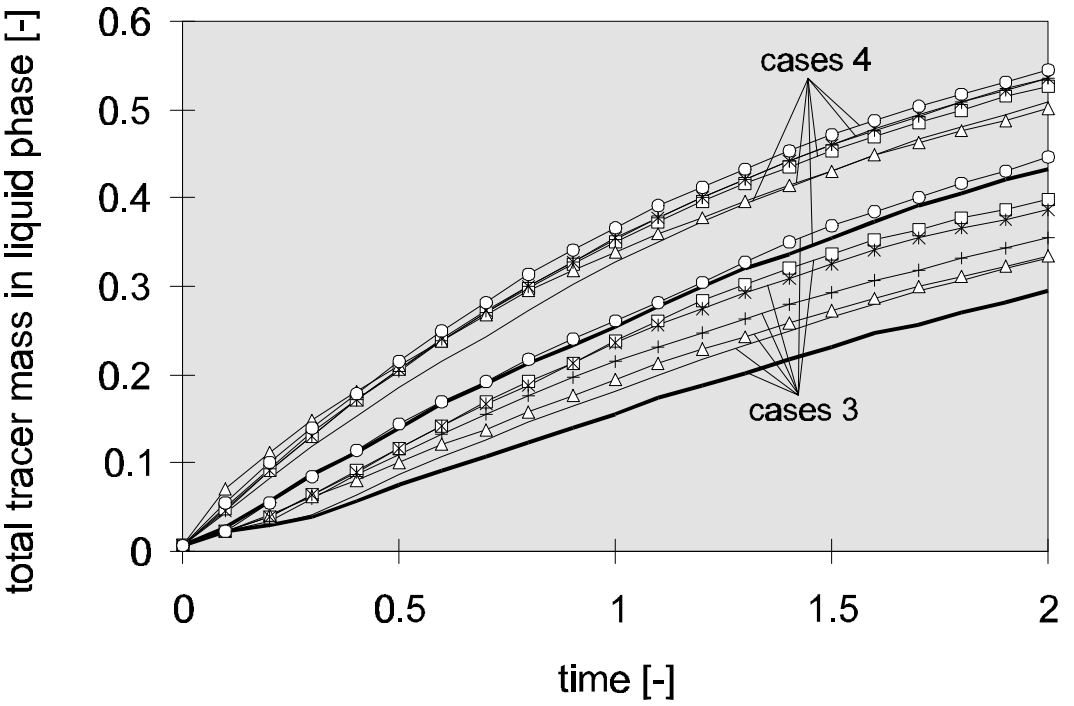

figure 17 *Total tracer mass in liquid phase as a function of time for cases A3-G3, and cases A4-G4.*
Legend: *case A;* *case B;* *case C;* *case D;* *case E;* *case F;* *case G*

First, an analysis for small Marangoni numbers and small time is presented. For these conditions, the growth of the maximum interface velocity with time is largest for intermediate Biot number. Consider a system in which diffusion is the main mass transfer mechanism, and, for clarity, no tracer component is present. Gradients in concentration of the surface tension determining solute parallel to the interface are reduced by mass flux parallel to the interface $J^{=}$. This (dimensionless) mass flux can be written in terms of the gas and liquid phase mass transfer coefficient parallel to the interface, $k_G^{=}$ and $k_L^{=}$:

$$J^{=} = \left(m\, k_G^{=} + k_L^{=}\right)\Delta c_i \qquad (40)$$

The concentration gradient parallel to the interface Δc_i is proportional to the mass flux normal to the interface, $J^{\perp}$.

$$J^{\perp} = m k_G^{\perp} c_i = \frac{m k_G^{\perp}}{1 + \dfrac{m k_G^{\perp}}{k_L^{\perp}}} \tag{41}$$

The largest concentration gradient parallel to the interface occurs when the ratio R of fluxes normal to the interface and parallel to the interface is maximal.

$$R = \frac{J^{\perp}}{J^{=}} = \frac{m k_G^{\perp}}{\left(1 + \dfrac{m k_G^{\perp}}{k_L^{\perp}}\right)\left(m k_G^{=} + k_L^{=}\right)} = \frac{1}{\dfrac{k_G^{=}}{k_G^{\perp}}\left(1 + Bi_R\right) + \dfrac{k_L^{=}}{k_L^{\perp}}\left(1 + \dfrac{1}{Bi_R}\right)} \tag{42}$$

The ratio R as a function of the average interfacial concentration is plotted in figure 18 for several values of the parameters $(k_G^{=}/k_G^{\perp})$ and $(k_L^{=}/k_L^{\perp})$. Interfacial concentration relates directly to Bi_R through equation (34).

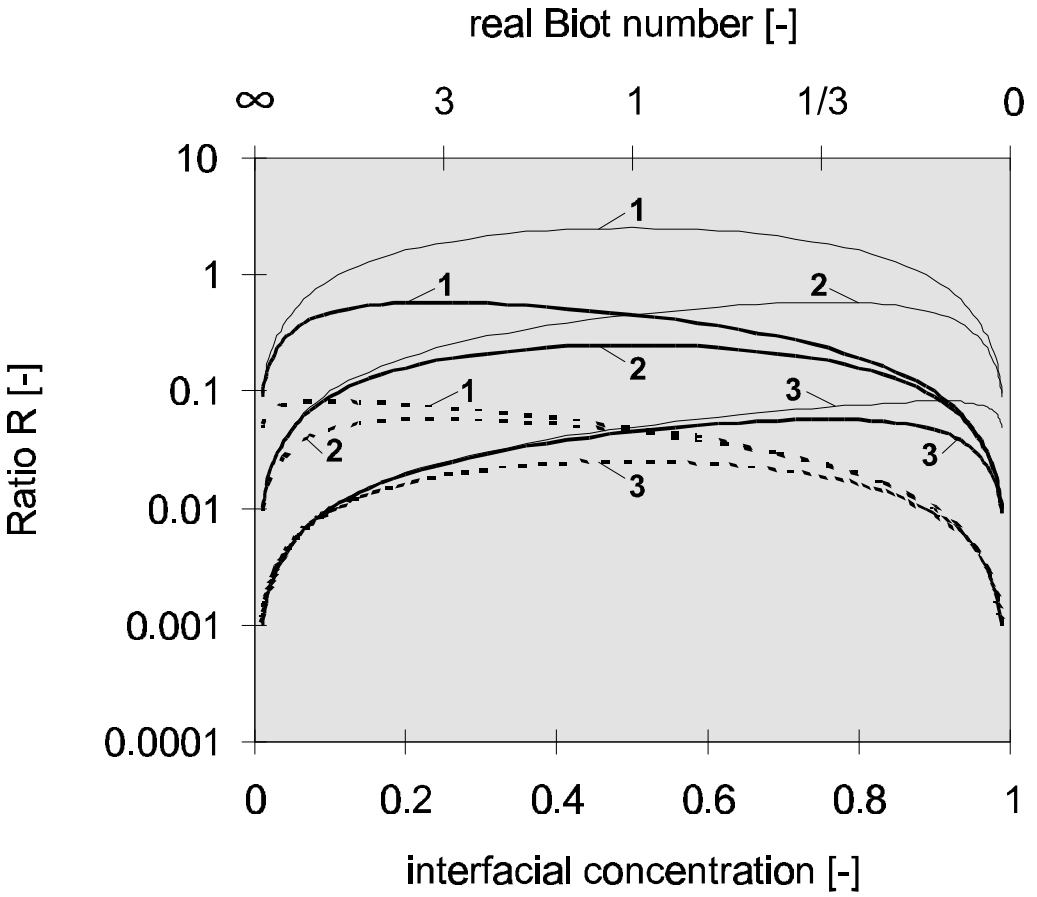

figure 18 *Ratio R as a function of interfacial concentration. Each curve corresponds to one value of $(k_G^{=}/k_G^{\perp})$ and one value of $(k_L^{=}/k_L^{\perp})$.*
*Legend: **1**: $(k_G^{=}/k_G^{\perp})$ = 0.1; **2**: $(k_G^{=}/k_G^{\perp})$ = 1; **3**: $(k_G^{=}/k_G^{\perp})$ = 10; ——— $(k_L^{=}/k_L^{\perp})$ = 0.1; ━━━ $(k_L^{=}/k_L^{\perp})$ = 1; - - - - $(k_L^{=}/k_L^{\perp})$ = 10*

Equation (42) expresses that when parameters $(k_G^{=}/k_G^{\perp})$ and $(k_L^{=}/k_L^{\perp})$ equal 1, the largest concentration gradients parallel to the interface, and therefore the largest interface velocities can be found for the case that $Bi_R = 1$, or $c_i = 0.5$. The maximum in R shifts to smaller Bi_R or larger c_i for larger ratios $(k_G^{=}/k_G^{\perp})/(k_L^{=}/k_L^{\perp})$ and to larger Bi_R or smaller c_i for smaller ratios $(k_G^{=}/k_G^{\perp})/(k_L^{=}/k_L^{\perp})$. The absolute value of R is smaller the larger $(k_G^{=}/k_G^{\perp})$ is and the larger $(k_L^{=}/k_L^{\perp})$ is.

Initially, both transport parallel and normal to the interface proceeds according to the penetration theory, i.e. $k_G^{=}/k_G^{\perp}$ and $k_L^{=}/k_L^{\perp}$ equal 1. After some time, mass transfer in the gas phase proceeds no longer according to the penetration theory, but more according to film theory. The length scale in the mass transfer coefficient equals the film thickness for transfer normal to the interface, and equals the length scale of a roll cell parallel to the interface (L). That is, $k_G^{=}/k_G^{\perp} = H_G/L$. For two roll cells, $k_G^{=}/k_G^{\perp} \approx 1.3$, while for 6 roll cells $k_G^{=}/k_G^{\perp} \approx 3.8$. For almost all cases A-G, $k_G^{=}/k_G^{\perp} > 1$, which implies that the maximum of R corresponds to a value somewhat larger than 0.5. In the liquid phase, diffusion is so slow for all cases except case C, that the penetration theory is valid throughout the calculation time. For case C, $k_L^{=}/k_L^{\perp}$ is a little larger than 1.

If for cases A1-G1, $k_G^{=}/k_G^{\perp}$ is set to 3.8 and $k_L^{=}/k_L^{\perp}$ to 1, except for case C, where $k_L^{=}/k_L^{\perp}$ = 1.5-2, the various growth factors in figures 5 and 14 can be explained qualitatively. In the diffusive regime, Bi_R grows in time. This implies that R increases when $Bi_R < 1$, but decreases when $Bi_R > 1$. This can be observed qualitatively in figure 5. In this figure, for Bi_N = 1.31, the growth factor of the Marangoni disturbance grows in time, while for Bi_N = 131 the growth factor reduces in time.

For larger Marangoni number and larger time, mass transfer in the liquid phase parallel and normal to the interface is controlled by convection. The analysis presented above does not hold, and a new analysis is presented here, partly along the same lines as presented by Golovin [9]. However, the gas phase is now also taken into account. Consider the system in figure 19.

The concentration of the surface tension determining solute of a fluid element which is transported along the interface from 1 to 2 only decreases when the flux of matter J_L from the liquid to the interface (between 1 and 2) is smaller than the flux of matter J_G away from the interface. Assume further that the mass transfer in the gas phase normal to the interface is not altered by the convection. The concentration gradient parallel to the interface induces a flux parallel to the interface, which serves to reduce this concentration difference. These fluxes should be balanced. That is,

$$J^{=} \propto \left(J_G - J_L\right) \tag{43}$$

$$J_G^{=} = k_G^{=}\left(c_{G,1} - c_{G,2}\right) \tag{44}$$

$$J_L^{=} \approx v_s\left(c_{L,1} - c_{L,2}\right) \tag{45}$$

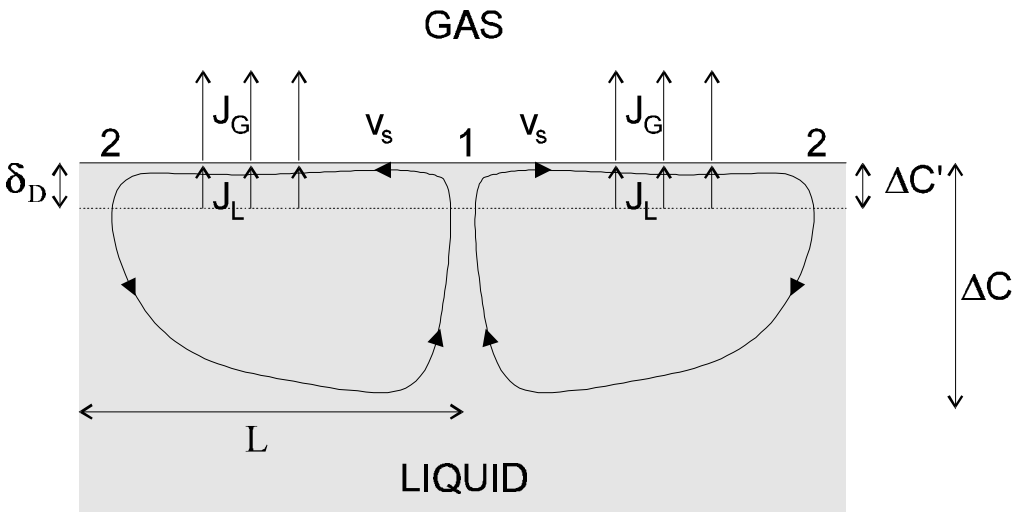

figure 19 The roll cell under consideration.

$$J^{=} \approx \left(v_s + m\,k_G^{=}\right)\left(c_{L,1} - c_{L,2}\right) \tag{46}$$

Combining equation (43) and (46) leads to:

$$\left(J_G - J_L\right) \propto \left(v_s + m\,k_G^{=}\right)\left(c_{L,1} - c_{L,2}\right) \tag{47}$$

The fluxes through the interface between points 1 and 2 can be expressed by the following correlations.

$$J_G = m\,k_G\,c_i = \frac{m\,k_G}{1 + \dfrac{m\,k_G}{k_L}} \tag{48}$$

$$J_L = k_L\,\Delta c' = b\,k_L^D\,\Delta c = b\,k_L^D\,\frac{\dfrac{m\,k_G}{k_L}}{1 + \dfrac{m\,k_G}{k_L}} \tag{49}$$

In the last equation, k_L^D is the liquid side mass transfer coefficient controlling the mass flux between the interface and δ_D, and b is an empirical parameter characterising the extent of surface renewal, as defined by Golovin. The mass transfer coefficient k_L^D can be expressed as:

$$k_L^D = \frac{D_L}{\delta_D} \tag{50}$$

The combination of equations (47), (48), and (49) leads to the following expression for the concentration difference:

$$c_1 - c_2 \propto \frac{1 - b\dfrac{k_L^D}{k_L}}{\dfrac{k_G^=}{k_G}\left(1 + Bi_R\right) + \dfrac{v_S}{k_L}\left(1 + \dfrac{1}{Bi_R}\right)} \qquad (51)$$

The right hand side of this equation behaves similarly as equation (42). As average velocities parallel to the interface are larger than average velocities normal to the interface, $v_S/k_L > 1$. For case G, v_S/k_L is considerably larger than for the other cases. This explains the small enhancement of mass transfer in case G, compared to the other cases (see figure 17). In the gas phase, velocities parallel to the interface are also much larger than normal to the interface, but in this phase diffusion still plays a significant role. Therefore, $(k_G^= / k_G^\perp)/(v_S/k_L) < 1$, and the maximum of R should be for $Bi_R > 1$. The parameter $(b\ k_L^D/k_L)$ is difficult to predict. The parameter b is very likely not independent of Bi_R and v_S, and neither is k_L^D/k_L.

With the considerations above in mind, it can be explained why enhancement of mass transfer is largest for real Biot numbers close to 1. Of course, one should keep in mind that the proposed models are highly simplified, and other effects should be considered as well, such as the dynamics of the system, numerical peculiarities, roll cell shape and size etc. Note, for example, that the model does not explain straightforwardly why the enhancement of mass transfer for case D4 is larger than for case E4. It is important, nevertheless, to stress that the model does provide a qualitative answer to most of the questions raised in this chapter.

In the literature cited in section 4.1, the influence of the real Biot number on the enlargement of the liquid side mass transfer coefficient has been mentioned by Brian et al. [2] and Semkov and Kolev [8]. Semkov and Kolev correlated wrongly calculated results by Imaishi et al. [5]. They tried to correlate the data by assuming that a larger concentration difference between bulk and interface would give a larger Marangoni effect. Therefore, they only tried to correlate n with the ratio $Bi_R^*/(1+Bi_R^*)$. Their correlation had small significance, and their findings can hardly be compared to the numerical results in this chapter. Note though that if $(k_G^= / k_G^\perp)/(v_S/k_L) << 1$, the concentration difference parallel to the interface in equation (51) becomes proportional to $Bi_R/(1+Bi_R)$:

$$c_1 - c_2 \propto \frac{\left(1 - b\dfrac{k_L^D}{k_L}\right)Bi_R}{\dfrac{v_S}{k_L}\left(1 + Bi_R\right)} \qquad (52)$$

Brian et al. studied three systems subject to Marangoni instability, i.e. acetone-water-air, diethyl ether-water-air, and triethylamine-water-air. Although they studied desorption in a wetted wall column, rather than in a quiescent layer, a qualitative comparison with the results in this chapter is justified. The systems Brian et al. studied varied predominantly in distribution coefficient. The results were correlated with equation (2). The parameter n was largest for the triethylamine system (real Biot numbers 0.29-0.43), smallest for the acetone system (real Biot numbers 0.05-0.08) and intermediate for the diethyl ether system (real Biot number 1.69-2.54).

That is, for the intermediate Biot number, the relative enhancement was largest. Although this seems a confirmation of the results in this chapter, one should consider that the triethylamine system possesses different properties (interfacial viscosity, Gibbs absorption) than the other systems, which makes direct comparison between the three systems difficult.

The roll cells in this study are regular, and their lifetime is much longer than the characteristic time of circulation. According to the definition of Golovin [9], these cells are type B roll cells. In deriving equations for the Sherwood number as a function of the ratio of resistances in the liquid and the gas phase (see the equations (17) and (18)), Golovin neglects the mass transport in the gas phase parallel to the interface. As a result of this assumption, Golovin does not predict that the closer the resistances in the two phases are together, the larger the Marangoni effect is, as equation (51) does. Rather, Golovin predicts that the Marangoni effect is largest when the concentration difference between the interface and the bulk is largest (i.e. when $Bi_R/(1+Bi_R)$ is largest). The results of this work show that this is not necessarily the case.

Furthermore, Golovin assumes that the parameter b and the roll cell size are independent of the Marangoni, Schmidt en Biot numbers. However, roll cell size and flow pattern can differ from case to case, and can depend on the mass transfer in the gas phase as well. This, for example, is the reason why the enhancement of mass transfer for case B4 is relatively large for small times (see figure 17).

Influence of the Marangoni number

The results of most experiments in literature and the theory of Golovin predict that the parameter n for the type of numerical experiments conducted in this study should be somewhere in the order of 0.2-0.5. Golovin predicts 0.33 for this parameter. From the results presented in this study, and specifically the results for the total tracer mass in the liquid phase as a function of time (figures, 4, 13, 17), it should be possible to determine a value for n. However, as the figures demonstrate, it is quite difficult to decide exactly how the value of n should be calculated. Different results are obtained depending on which time after the start of the experiment the results are compared. Equation (2) is obviously too simple to summarise the results in this chapter. An estimate for n is made, nevertheless.

It has been decided to use only the results of the cases A3-G3 and A4-G4, as the critical times for the A2-G2 cases were much longer than for the former cases which makes comparison difficult. Furthermore, only an average k_L value was calculated, based on the value of the total tracer mass in the liquid phase at t = 2. In this way, the effect demonstrated by case B4 (initially a steep curve, later much less steep) is smoothed out. To calculate the value of k_L, the following formula was used.

$$\frac{M_\zeta}{M_{\zeta,max}} = \left(1 - e^{-\frac{k_L H_L}{\nu} t}\right) \qquad (53)$$

In this equation, M_ζ and $M_{\zeta,max}$ are the total dimensionless tracer mass in the container, and the maximum total tracer mass in the container ($M_{\zeta,max} = \pi/4$). To calculate n for each case A-G, the Marangoni numbers $Ma_{G,L}$ are calculated as an average of $Ma_{G,L}$ in time. That is, after each 400 time steps (one tenth of total time), the average interfacial concentration is computed and used to calculate $Ma_{G,L}$. These ten values of $Ma_{G,L}$ are subsequently averaged to obtain an overall average value of $Ma_{G,L}$. For each case, two $Ma_{G,L}$ - k_L combinations are found, and from these combinations, values for n are calculated. In this way, for each of the cases A-G one value for n is found. The accuracy of n is admittedly small, but the resulting values of n are only used to obtain an insight in the order of magnitude. In table 2, the results of the calculations are summarised.

Table 2. Values of n for the different cases.

Case	average k_L [m/s]	average $Ma_{G,L}$ [-]	n
Case A3	$2.8\ 10^{-5}$	$2.4\ 10^{4}$	0.31
Case A4	$5.2\ 10^{-5}$	$1.8\ 10^{5}$	
Case B3	$2.8\ 10^{-5}$	$2.4\ 10^{4}$	0.26
Case B4	$5.1\ 10^{-5}$	$2.3\ 10^{5}$	
Case C3	$3.0\ 10^{-5}$	$9.8\ 10^{3}$	0.32
Case C4	$5.7\ 10^{-5}$	$7.4\ 10^{4}$	
Case D3	$4.2\ 10^{-5}$	$1.6\ 10^{5}$	0.15
Case D4	$5.9\ 10^{-5}$	$1.6\ 10^{6}$	
Case E3	$3.5\ 10^{-5}$	$6.7\ 10^{5}$	0.20
Case E4	$5.6\ 10^{-5}$	$6.5\ 10^{6}$	
Case F3	$3.4\ 10^{-5}$	$6.8\ 10^{5}$	0.23
Case F4	$5.7\ 10^{-5}$	$6.5\ 10^{6}$	
Case G3	$2.3\ 10^{-5}$	$5.4\ 10^{6}$	0.24
Case G4	$4.0\ 10^{-5}$	$5.2\ 10^{7}$	

The values of n found in this study are in the same range as the experimental values found in literature. All the values of n are smaller than 0.33, which is the value Golovin predicted. There are several reasons for this discrepancy. For example, Golovin did not take into account that roll cell size can depend on the Marangoni number, as was demonstrated in this study. For larger Marangoni number, the ratio (H/L) in equation (12) therefore diminishes, and the apparent value of n is therefore smaller.

Another source of error in Golovins consideration is his contention that the concentration difference (c_1 - c_2) is equal to $\Delta c'$ (see equation (4) in his paper). The numerical results demonstrate that the concentration difference parallel to the interface is not the same as the concentration difference across the boundary layer. In figure 16b, for example, the maximum

difference in interface concentration is 0.006, while the difference in concentration across the boundary layer is approximately 0.46.

Influence of the Schmidt numbers

The influence of the liquid phase Schmidt number on the enhancement of the liquid side mass transfer coefficient is expressed by equation (22). Since the Schmidt number in this study was only varied by changing the liquid phase diffusion coefficient, and not the liquid phase kinematic viscosity, the formula can best be rewritten as:

$$k_L = b^{4/3} \left(Ma_{G,L}^{n}\right)^{1/3} Sc^{-1/2} \left(\frac{H_L}{L}\right)^{2/3} \left(\frac{\nu}{H_L}\right) \qquad (54)$$

The equation should apply to the solute as well as to the tracer. The equation demonstrates that for the cases studied in this chapter, the enhancement of the liquid phase mass transfer coefficient is larger the smaller the Schmidt number is (at a constant ratio Ma/Sc_L). When the cases A4, B4, and C4 are compared, one finds that the enhancement is indeed largest for the case with the smallest liquid phase Schmidt number (C4), other parameters (Ma/Sc_L and Bi_N) being equal. Similarly, if cases E4, F4, and G4 are compared, the enhancement is smallest for the case with the largest liquid phase Schmidt number.

Although the results compare qualitatively to equation (54), table 2 demonstrates that k_L is not inversely proportional to the square root of the Schmidt number. Discrepancy is among other things caused by the fact that equation (54) has been derived under the assumption that mass transfer in the liquid phase is always determined by the intensity of the convection, whatever the value of the Marangoni number. In reality, for small Ma, diffusion determines the mass transfer rate. Furthermore, not all the assumptions made by Golovin are justified, as discussed before.

Equation (54) can also be used to explain the results in section 4.5 qualitatively. In this section, it was found that the smallest enhancement of mass transfer was found for the largest Schmidt number, and the largest enhancement for the intermediate Schmidt number. These results can be explained as a combination of the effect caused by the absolute value of the real Biot number, and the effect expressed by equation (54).

The influence of the gas phase Schmidt number is not discussed beyond the argument already presented in section 4.4, as no literature is available with which the results can be compared.

4.7 Conclusions

The most important conclusions of the study presented in this chapter are:

1. The addition of a tracer component to the system studied in chapter 3 gives good insight into the influence of Marangoni convection on mass transfer.
2. The value of the real Biot number largely determines the effect of Marangoni convection on the mass transfer coefficient, given a value of Ma/Sc_L. If mass transfer resistance is located mainly in one of the phases, mass transfer in the other phase cancels out any concentration gradients parallel to the interface. In other words, if the real Biot number, i.e. the mass transfer resistance ratio, has a value close to one, the enhancement of the mass transfer coefficient is largest. This conclusion contradicts the impression quite often given in literature that the Marangoni effect is larger the larger the real Biot number is.
   A semi-quantitative model has been developed to support these results. It proved to be essential to take the mass transfer parallel to the interface in both liquid and gas phase into account.
3. The value for the parameter n (equation (2)) in this study (0.15-0.32) differs from case to case, and depends on time, Biot number, liquid phase and gas phase Schmidt numbers. The values are close to the values found in experimental studies, and the value predicted by the theoretical study of Golovin. Several explanations for the discrepancy between the results and the theory of Golovin are proposed. Equation (2) can not describe all the results in this chapter.
4. It is very difficult to generalise the results in this chapter to correlations, which can be used by chemical engineers to predict the liquid side mass transfer coefficient. This is caused by the large number of parameters that influence the Marangoni effect. Furthermore, in actual gas-liquid mass transfer systems, additional parameters, such as Gibbs adsorption and interfacial viscosity also play a role. The results in this chapter do, however, give more insight in the mechanisms involved.

List of symbols

b	surface renewal parameter introduced in equation (9)	[-]
Bi_N	numerical Biot number (see chapter 3, equation (23))	[-]
Bi_R	real Biot number (equation (31))	[-]
c	concentration	[kg m^{-3}] or [-]
C_{max}	maximum concentration contour line (used in figures)	[-]
d	penetration depth	[m]
D	diffusion coefficient	[m^2 s^{-1}]
H	characteristic length	[m]
H_G	size of gas phase (see chapter 3)	[m]
H_L	size of liquid phase (see chapter 3)	[m]
i	label for grid point (θ co-ordinate)	
j	mass flux through the interface	[kg m^2 s^{-1}]
J	flux of dimensionless mass	[m s^{-1}]
j	label for grid point	
k	mass transfer coefficient	[m s^{-1}]
k_L^D	mass transfer coefficient between interface and δ_D	[m s^{-1}]
K	empirical parameter (equation (3))	
L	characteristic length scale of roll cell	[m]
m	distribution coefficient	[kg m^{-3} kg^{-1} m^3]
M	total dimensionless mass in container	[-]
m_B	parameter defined in equation (18)	[-]
Ma	Marangoni number	[-]
Ma_B	Marangoni number defined by Brian (equation (4))	[-]
$Ma_{G,L}$	Marangoni number defined by Golovin (equation (11))	[-]
$Ma_{G,L}^0$	initial Golovin Marangoni number (equation (15))	[-]
$Ma_{G,L}^n$	modified Golovin Marangoni number (equation (20))	[-]
Ma_{Gr}	Marangoni number defined by Grymzin (5)	[-]
Ma_W	Marangoni number defined by Warmuzinski (eq. (6))	[-]
n	parameter defined by equation (2)	[-]
N_{dist}	parameter defined in chapter 3	[-]
N_P	integer, denoting size of convex container (chapter 3)	[-]
N_t	number of time steps	[-]
N_{wG}	number of grid points in w-direction (gas phase)	[-]
N_{wL}	number of grid points in w-direction (liquid phase)	[-]
N_θ	number of grid points in θ-direction	[-]
Pe	Peclet number	[-]
r	radial co-ordinate	[-]
r	phase resistance ratio defined in equation (16)	[-]
R	ratio of fluxes normal and parallel to interface	[-]
S_B	function defined by equation (19)	[-]

Sc	Schmidt number	[-]
Sh	Sherwood number	
t	time	[-]
v_S	interfacial velocity in roll cell (see figure 19)	[m s^{-1}]
x	length co-ordinate	[-]
X_{dist}	parameter defined in chapter 3	[-]
γ	surface tension	[N m^{-1}]
δ	penetration depth	[-]
δ_D	depth from interface as defined in figure 19	[-]
Δ_C	distance between concentration contour lines (figures)	[-]
$\Delta c'$	concentration gradient defined in figure 19	[-]
Δ_S	distance between stream function contour lines (figures)	[-]
ε	parameter defined in chapter 3	[-]
ζ	tracer concentration	[-]
μ	dynamic viscosity	[Pa s]
ν	kinematic viscosity	[m^2 s^{-1}]
ϕ	enhancement factor defined by equation (1)	
ψ	stream function	[-]

Subscripts

B	bulk
C	critical
G	gas phase
i	interface
L	liquid phase
P	phase (gas or liquid)
0	initial
ζ	tracer

Superscripts

0	initial
*	in the absence of Marangoni convection
=	parallel to interface
$\perp$	normal to interface

Literature

[1] M.W. Clark, C.J. King, "Evaporation rates of volatile liquids in a laminar flow system. Part II. Liquid mixtures", A.I.Ch.E. J., 16 (10), 69-75, 1970

[2] P.L.T. Brian, J.E. Vivian, S.T. Mayr, "Cellular convection in desorbing surface tension-lowering solutes from water", Ind. Eng. Chem. Fundam., 10 (1), 75-83, 1971

[3] K. Fujinawa, M. Hozawa, N. Imaishi, "Effects of desorption and absorption of surface tension-lowering solutes on liquid-phase mass transfer coefficients at a turbulent gas-liquid interface", J. Chem. Eng. Japan, 11 (2), 107-111, 1978

[4] H.W. van der Klooster, A.A.H. Drinkenburg, "The influence of gradients in surface tension on the mass transfer in a packed column", Inst. Chem. Engrs Symp. Series, no. 56, 2.5/21-2.5/37, 1979

[5] N. Imaishi, Y. Suzuki, M. Hozawa, K. Fujinawa, "Interfacial turbulence in gas-liquid mass transfer", Int. Chem. Eng., 22 (4), 659-665, 1982

[6] Y.N. Grymzin, S.Y. Kvashnin, V.A. Lotkhov, V.A. Malyusov, "A method for taking into account the effect of surface tension gradient in calculating the kinetics of rectification in packed or film columns", transl. from: Teoreticheskie Osnovy Khimicheskoi Tekhnologii, 16 (5), 579-584, 1982

[7] K. Warmuzinski, J. Buzek, "A model of cellular convection during absorption accompanied by chemical reaction", Chem. Eng. Sci., 45 (1), 243-254, 1990

[8] K. Semkov, N. Kolev, "On the evaluation of the interfacial turbulence (the Marangoni effect) in gas (vapour)-liquid mass transfer. Part I. A method for estimating the interfacial turbulence effect", Chem. Eng. Process., 29, 77-82, 1991

[9] A.A. Golovin, "Mass transfer under interfacial turbulence: kinetic regularities", Chem. Eng. Sci., 47 (8), 2069-2080, 1992

[10] L.M. Rabinovich, "Problems in modelling and intensification of mass transfer with interfacial instability and self-organization", Ch. 4 in "Mathematical Modelling of Chemical Processes" by L.M. Rabinovich, (transl. from Russian), CRC Press, Boca Raton, 289-417, 1992

[11] P.L.T. Brian, J.R. Ross, "The effect of Gibbs adsorption on Marangoni instability in penetration mass transfer", A.I.Ch.E. J., 18 (3), 582-591, 1972

[12] H.A. Dijkstra, "Mass transfer induced convection near gas-liquid interfaces", Ph.D. Thesis, University of Groningen, 1988

[13] C.V. Sternling, L.E. Scriven, "Interfacial turbulence: hydrodynamic instability and the Marangoni effect", A.I.Ch.E. J., 5 (4), 514-523, 1959